Reports on Progress in Physics

Observation of $\gamma\gamma \to \tau\tau$ in proton–proton collisions and limits on the anomalous electromagnetic moments of the τ lepton

OPEN ACCESS
IOP Publishing
Reports on Progress in Physics
Rep. Prog. Phys. **87** (2024) 107801 (33pp)
https://doi.org/10.1088/1361-6633/ad6fcb

Observation of $\gamma\gamma \to \tau\tau$ in proton–proton collisions and limits on the anomalous electromagnetic moments of the τ lepton

The CMS Collaboration

CERN, Geneva, Switzerland

E-mail: cms-publication-committee-chair@cern.ch

Received 6 June 2024, revised 23 July 2024
Accepted for publication 15 August 2024
Published 2 September 2024

Corresponding editor: Dr Lorna Brigham

Abstract

The production of a pair of τ leptons via photon–photon fusion, $\gamma\gamma \to \tau\tau$, is observed for the first time in proton–proton collisions, with a significance of 5.3 standard deviations. This observation is based on a data set recorded with the CMS detector at the LHC at a center-of-mass energy of 13 TeV and corresponding to an integrated luminosity of 138 fb^{-1}. Events with a pair of τ leptons produced via photon–photon fusion are selected by requiring them to be back-to-back in the azimuthal direction and to have a minimum number of charged hadrons associated with their production vertex. The τ leptons are reconstructed in their leptonic and hadronic decay modes. The measured fiducial cross section of $\gamma\gamma \to \tau\tau$ is $\sigma^{\text{fid}}_{\text{obs}} = 12.4^{+3.8}_{-3.1}$ fb. Constraints are set on the contributions to the anomalous magnetic moment (a_τ) and electric dipole moments (d_τ) of the τ lepton originating from potential effects of new physics on the $\gamma\tau\tau$ vertex: $a_\tau = 0.0009^{+0.0032}_{-0.0031}$ and $|d_\tau| < 2.9 \times 10^{-17}\, e\,\text{cm}$ (95% confidence level), consistent with the standard model.

Keywords: CMS, exclusive production, taus

1. Introduction

The production of lepton pairs via photon–photon fusion in proton–proton (pp) collisions draws significant interest since it is a pure quantum electrodynamics (QED) process at leading order, for which the theoretical cross section can be calculated with uncertainties below 1% [1]. If both protons remain intact after their electromagnetic interaction, the final state has a particularly clean topology characterized by two leptons emitted back-to-back in azimuth and without any hadronic activity surrounding it. Although the photon-fusion production of dileptons in hadronic collisions has been measured precisely for electrons and muons [2–8], a similar experimental precision is lacking for τ leptons [9, 10]. The photon-fusion channel has long been proposed to probe the $\gamma - \tau$ coupling at hadron colliders [11–14], because the short τ lepton lifetime makes other measurements difficult.

The most general form of photon–lepton coupling ($ie\Gamma^\mu$) satisfying Lorentz invariance is:

$$\Gamma^\mu = \gamma^\mu F_1\left(q^2\right) + \frac{\sigma^{\mu\nu} q_\nu}{2m}\left[iF_2\left(q^2\right) + F_3\left(q^2\right)\gamma_5\right], \qquad (1)$$

where $\sigma^{\mu\nu} = i[\gamma_\mu, \gamma_\nu]/2$ is the spin tensor proportional to the commutator of the gamma matrices, q is the momentum transfer between incoming and outgoing leptons of mass m, and $F_i\left(q^2\right)$ $(i = 1,2,3)$ are form factors that contain the complete information about the electric and magnetic couplings of the lepton. Beyond serving as a sensitive test of QED interactions, the photon–photon production process also offers insights into the anomalous electromagnetic moments of the lepton $(\ell = \mathrm{e}, \mu, \tau)$, $F_2(0) = a_\ell \equiv (g_\ell - 2)/2$ and $F_3(0) = -2m d_\ell / e$, and is a powerful probe of physics beyond the standard model (BSM). In this expression, the gyromagnetic ratio g_ℓ is a constant term that relates the magnetic moment of the lepton to its spin, and d_ℓ is the lepton anomalous electric dipole moment. The one-loop contribution to a_ℓ is equal to the so-called 'Schwinger term', which is common to all leptons [15]:

$$a_\ell = \frac{\alpha}{2\pi} \simeq 0.001\,16, \tag{2}$$

where α is the fine-structure constant.

The anomalous magnetic moment of the electron has been measured to agree with the standard model (SM) with an impressive precision of twelve significant digits [16, 17]. Measurements of a_μ by the Muon g-2 Collaboration reach a precision of ten significant digits and appear in conflict with certain theoretical predictions [18–20]. If BSM effects scale with the squared lepton mass, deviations of a_τ from the SM predictions would be more than two orders of magnitude larger than they are for a_μ. The photon-fusion production of a pair of τ leptons probes the $\tau\tau\gamma$ vertex and can be used to measure a_τ, which is predicted to be $a_\tau = 1.17721 \pm 0.00005 \times 10^{-3}$ in the SM [21]. This same process can also be studied to constrain d_τ, which, since there is no appreciable violation of charge-conjugation and parity symmetries in the charged lepton sector of the SM, is predicted to have a nonzero but tiny value [22].

The signal in this analysis is $\mathrm{pp} \xrightarrow{\gamma\gamma} \mathrm{p}^{(*)}\tau^+\tau^-\mathrm{p}^{(*)}$, where $\mathrm{p}^{(*)}$ denotes a final-state proton that stays intact or fragments after the photon emission. When both protons radiate coherently a photon and remain intact after their interaction, the process is called exclusive or elastic. Since the protons do not dissociate, these events are characterized by the absence of any hadron produced, other than those from the τ lepton decays. The photons emitted in the elastic processes are almost on-shell, limiting their virtuality to small values $(q^2 \to 0)$ [1], and the produced τ leptons are back-to-back in the azimuthal direction. When one or both incoming protons fragment as a result of photon emission, the process is called either single- or double-dissociative. Single- and double-dissociative events can also give rise to an elastic-like signature when the proton remnants are not reconstructed because they fall outside of the detector acceptance. Figure 1 shows the three diagrams considered here, contributing to the $\gamma\gamma \to \tau\tau$ process in pp collisions.

The $\gamma\gamma \to \tau\tau$ process has been observed by the ATLAS and CMS Collaborations in ultraperipheral collisions of lead ions [9, 10], and used to set constraints on a_τ. The observation was driven by signal events with a di-τ invariant mass, $m_{\tau\tau}$, typically below 20 GeV. This paper describes the first measurement of the photon-fusion production of a pair of τ leptons in pp collisions. Because of the trigger requirements, experimentally accessible signal events have $m_{\tau\tau} > 50\,\mathrm{GeV}$. The $\tau\tau$ production in this phase space has a much lower cross section, but the integrated luminosity is much higher than the one achievable with heavy ion collisions at the LHC. Additionally, BSM effects from new heavy particles [23] are enhanced at high mass, and the phase space accessible in pp collisions is more sensitive to BSM scenarios with non-SM a_τ and d_τ values than that accessible in ultraperipheral collisions of lead ions. Outside of LHC experiments, constraints on a_τ were previously set by the DELPHI, OPAL, and L3 experiments [24–26]. Constraints on d_τ were determined by the Belle, L3, OPAL, and ARGUS Collaborations [25–28].

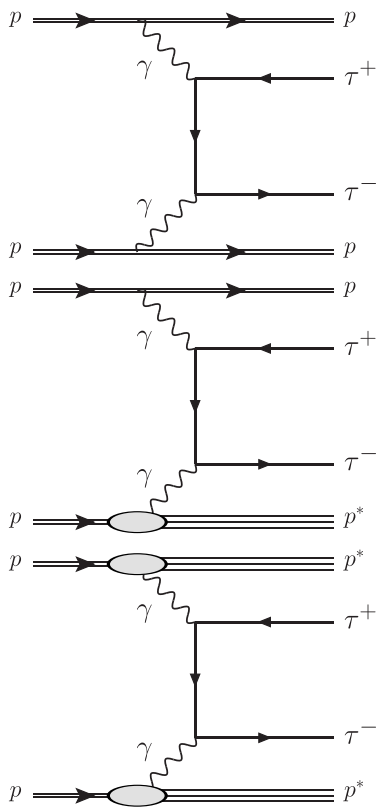

Figure 1. Feynman diagrams for the production of τ lepton pairs by photon–photon fusion. The exclusive (upper), single proton dissociation (middle), and double proton dissociation (lower) topologies are shown.

This paper is based on pp collision data at $\sqrt{s} = 13\,\mathrm{TeV}$ collected with the CMS detector in 2016–2018, corresponding to an integrated luminosity of 138 fb^{-1}. To select the signal, we apply so-called exclusivity criteria, which rely on the kinematics of the di-τ system and on the activity in the tracker part of the detector around the di-τ vertex. In particular, by selecting events with no track within 0.1 cm of the di-τ vertex, we

can reduce the background contributions by about three orders of magnitude for a signal efficiency of around 50%. Such a strategy has been used previously to identify similar photon–photon processes in pp collisions [8, 29–33]. Four different final states, corresponding to different decay modes of the τ leptons, are studied to measure the signal strength: eμ, eτ_h, $\mu\tau_h$, and $\tau_h\tau_h$, where τ_h denotes a τ lepton decaying hadronically. Events with two reconstructed muons are used to derive corrections to the simulated samples. The visible mass of the τ candidates, m_{vis}, computed as the invariant mass of the visible decay products of the two τ leptons, is used as a biased estimator of $m_{\tau\tau}$ to extract the significance of the signal and set constraints on a_τ and d_τ. Tabulated results are provided in the HEPData record for this analysis [34].

2. The CMS detector

The central feature of the CMS apparatus is a superconducting solenoid of 6 m internal diameter, providing a magnetic field of 3.8 T. Within the solenoid volume are a silicon pixel and strip tracker, a lead tungstate crystal electromagnetic calorimeter (ECAL), and a brass and scintillator hadron calorimeter (HCAL), each composed of a barrel and two endcap sections. Forward calorimeters extend the pseudorapidity coverage provided by the barrel and endcap detectors. Muons are measured in gas-ionization detectors embedded in the steel flux-return yoke outside the solenoid. A more detailed description of the CMS detector, together with a definition of the coordinate system used and the relevant kinematic variables, is presented in [35].

Events of interest are selected using a two-tiered trigger system. The first level, composed of custom hardware processors, uses information from the calorimeters and muon detectors to select events at a rate of around 100 kHz within a fixed latency of 4 μs [36]. The second level, known as the high-level trigger, consists of a farm of processors running a version of the full event reconstruction software optimized for fast processing, and reduces the event rate to around 1 kHz before data storage [37].

3. Signal and background modeling

Signal samples corresponding to the elastic photon-fusion production of a τ lepton pair are generated using the GAMMA-UPC generator [38], which is implemented in the MADGRAPH5_aMC@NLO v3.5 code [39–42], including the initial photon k_T effects . The GAMMA-UPC generator derives photon fluxes from electric dipole and charge form factors for protons and ions, and includes realistic hadronic survival probabilities for them.

The photon fluxes used here are those derived from the elastic charge form factor of the proton. Samples generated with the SUPERCHIC 4 generator [43] are used as a cross-check, as described in section 7.

In this analysis, a_τ and d_τ are parameterized in MADGRAPH5_aMC@NLO using the SMEFTsim package [44, 45], as suggested in [14]. The corresponding BSM Lagrangian in the SM effective field theory (SMEFT) approach consists of two dimension-6 operators modifying a_τ and d_τ at tree level:

$$\mathcal{L}_{\text{BSM}} = \frac{C_{\tau B}}{\Lambda^2}\bar{L}_L\sigma^{\mu\nu}\tau_R H B_{\mu\nu} + \frac{C_{\tau W}}{\Lambda^2}\bar{L}_L\sigma^{\mu\nu}\tau_R\sigma^i H W^i_{\mu\nu} + \text{h.c.}, \quad (3)$$

where Λ is the scale of BSM physics, L_L represents the left-handed τ lepton doublet, τ_R corresponds to the right-handed τ lepton, H is an SU(2) scalar doublet, $B_{\mu\nu}$ is the weak hypercharge field, $W^i_{\mu\nu}$ represents the weak isospin field, and $C_{\tau B}$ and $C_{\tau W}$ are the Wilson coefficients. Using the SMEFTsim_general_alphaScheme_UFO model [44, 45], after electroweak symmetry breaking, the $\tau\tau\gamma$ vertex is parameterized as:

$$V_{\tau\tau\gamma} = ie\gamma^\mu - \frac{v\sqrt{2}}{\Lambda^2}\left[\text{Re}\left[C_{\tau\gamma}\right] + \text{Im}\left[C_{\tau\gamma}\right]i\gamma_5\right]\sigma^{\mu\nu}q_\nu, \quad (4)$$

where $C_{\tau\gamma} = \cos\theta_W C_{\tau B} - \sin\theta_W C_{\tau W}$, $v \approx 246\,\text{GeV}$ is the Higgs vacuum expectation value, and θ_W is the weak mixing angle. Using equations (1) and (4), deviations from the SM predictions of a_τ and d_τ can be expressed as:

$$\delta a_\tau = \frac{2m_\tau}{e}\frac{\sqrt{2}v}{\Lambda^2}\text{Re}\left[C_{\tau\gamma}\right] \quad (5)$$

and

$$\delta d_\tau = \frac{\sqrt{2}v}{\Lambda^2}\text{Im}\left[C_{\tau\gamma}\right]. \quad (6)$$

For simplicity and without loss of generality, since δa_τ and δd_τ only depend on the linear combination of $C_{\tau W}$ and $C_{\tau B}$, we set $C_{\tau W}$ to 0 in the signal simulation. The coefficient $C_{\tau B}$ alone is modified to simulate different $C_{\tau\gamma}$ values, which can be reinterpreted as linear combinations of $C_{\tau W}$ and $C_{\tau B}$. The BSM contributions to the $Z \to \tau\tau$ vertex cancel for $C_{\tau W} = -\tan\theta_W C_{\tau B}$, but other values of $C_{\tau W}$ would result in variations in the Drell–Yan (DY) process prediction that are negligible with respect to the systematic uncertainties of this background, which are described in section 9. The simulation of different anomalous electromagnetic moments is performed using matrix element reweighting [46], scanning over a range of $C_{\tau B}$ values. In the simulation, we set Λ to 2 TeV, but the results were verified to be independent of the scale of new physics. Since the anomalous electromagnetic moments of the τ lepton depend on a linear combination of $C_{\tau W}/\Lambda^2$ and $C_{\tau B}/\Lambda^2$, the analysis results can also be interpreted in this two-dimensional plane. The form factor formalism of equation (1) and the SMEFT approach are equivalent assuming $q^2 = 0$.

The GAMMA-UPC generator is also used to simulate the elastic photon-fusion production of pairs of electrons, muons, and W bosons, which are backgrounds in the signal region (SR). Single- and double-dissociative processes are not simulated but estimated from data as described later.

The MADGRAPH5_aMC@NLO 2.6.5 event generator is used to generate events originating from the $Z/\gamma^* + \text{jets}$

and W + jets processes, as well as from diboson production with two leptons and two neutrinos in the final state. These processes are simulated at next-to-leading order (NLO) with the FxFx jet matching and merging [41]. The MadGraph5_aMC@NLO generator is also used for the simulation of the minor contribution from other diboson production events, whereas POWHEG 2.0 [47–51] is used for $\mathrm{t\bar{t}}$ and single top quark production. The generators are interfaced with PYTHIA 8.240 [52] to model parton showering and hadronization, the underlying event activity, as well as the decay of the τ leptons. The PYTHIA parameters affecting the description of the underlying event are set to the CP5 tune [53]. The NNPDF3.1 parton distribution function (PDF) set [54–56] at next-to-NLO accuracy is used for background simulations. Additional pp interactions per bunch crossing (pileup) are added to the simulated samples with a distribution that is chosen to match that observed in the data. Generated events are processed through a GEANT4 [57] simulation of the CMS detector.

4. Object reconstruction

The global event reconstruction (also called particle-flow event reconstruction [58]) aims to reconstruct and identify each particle in an event, with an optimized combination of all subdetector information. In this process, the identification of the particle type (photon, electron, muon, charged hadron, or neutral hadron) plays an important role in the determination of the particle direction and energy. Photons are identified as ECAL energy clusters not linked to the extrapolation of any charged particle trajectory to the ECAL. Electrons are identified as a primary charged-particle track and potentially many ECAL energy clusters corresponding to this track extrapolation to the ECAL and to possible bremsstrahlung photons emitted along the way through the tracker material. Muons are identified as tracks in the central tracker consistent with either a track or several hits in the muon system and associated with calorimeter deposits compatible with the muon hypothesis. Charged hadrons are identified from the charged-particle tracks that are not associated with electrons or muons. Finally, neutral hadrons are identified as HCAL energy clusters not linked to any charged-hadron trajectory, or as a combined ECAL and HCAL energy excess with respect to the expected charged-hadron energy deposit.

The electron momentum is estimated by combining the energy measurement in the ECAL with the momentum measurement in the tracker. The momentum resolution for electrons with transverse momentum $p_T \approx 45\,\mathrm{GeV}$ from $Z \to ee$ decays ranges 1.6%–5.0%. It is generally better in the barrel region than in the endcaps, and also depends on the bremsstrahlung energy emitted by the electron as it traverses the material in front of the ECAL [59, 60].

Muons are measured in the pseudorapidity range $|\eta| < 2.4$, with detection planes made using three technologies: drift tubes, cathode strip chambers, and resistive-plate chambers. The efficiency to reconstruct and identify muons is greater than 96%. Matching muons to tracks measured in the silicon tracker results in a relative p_T resolution of 1% in the barrel and 3% in the endcaps for muons with p_T up to 100 GeV [61].

Hadronic τ lepton decays (τ_h) are reconstructed from jets, using the hadrons-plus-strips algorithm [62], which combines 1 or 3 tracks with energy deposits in the calorimeters clustered as strips. Neutral pions are reconstructed as strips with dynamic size in η-ϕ (where ϕ is the azimuthal angle in radians) from reconstructed electrons and photons, where the strip size varies as a function of the p_T of the electron or photon candidate. The τ_h candidates are reconstructed in four possible decay modes (DMs): a single charged hadron ($h^{\pm}$), a charged hadron with at least one neutral pion ($h^{\pm} + \pi^0(s)$), three charged hadrons with no neutral pion ($h^{\pm}h^{\mp}h^{\pm}$), or 3 charged hadrons with at least one neutral pion ($h^{\pm}h^{\mp}h^{\pm} + \pi^0(s)$). To distinguish genuine τ_h decays from jets originating from the hadronization of quarks or gluons, and from electrons or muons, the DEEPTAU algorithm [63] is used. Information from all individual reconstructed particles near the τ_h axis is combined with properties of the τ_h candidate in the event. The tight working point is used to separate τ_h candidates from jets; its efficiency is about 65% for τ_h with $20 < p_T < 100\,\mathrm{GeV}$ [63]. The loosest working point, used in the background estimation procedure, has an efficiency above 98%. The rate of a jet to be misidentified as τ_h by the DEEPTAU algorithm depends on the p_T and quark flavor of the jet. In simulated events from W boson production in association with jets, it has been estimated to be below the percent level for the tight working point. The misidentification rate for electrons (muons) is 2.60 (0.03)% for a genuine τ_h identification efficiency of 80 (>99)%.

The missing transverse momentum vector $\vec{p}_T^{\,\mathrm{miss}}$ is computed as the negative vector p_T sum of all the particle-flow candidates in an event, and its magnitude is denoted as p_T^{miss} [64]. The $\vec{p}_T^{\,\mathrm{miss}}$ is modified to correct the energy scale of the reconstructed jets in the event. Anomalous high-p_T^{miss} events can be due to a variety of reconstruction failures, detector malfunctions or noncollision backgrounds. Such events are rejected by event filters that are designed to identify more than 85%–90% of the spurious high-p_T^{miss} events with a mistagging rate less than 0.1% [64].

Tracks with $p_T > 0.5\,\mathrm{GeV}$ and $|\eta| < 2.5$ are used in this analysis to measure the hadronic activity in the event. The silicon tracker used in 2016 measured charged particles within the range $|\eta| < 2.5$. For nonisolated particles of $1 < p_T < 10\,\mathrm{GeV}$ and $|\eta| < 1.4$, the track resolutions were typically 1.5% in p_T and 25–90 (45–150) μm in the transverse (longitudinal) impact parameter [65]. At the start of 2017, a new pixel detector was installed [66]; the upgraded tracker measured particles up to $|\eta| < 3.0$ with typical resolutions of 1.5% in p_T and 20–75 μm in the transverse impact parameter [67] for nonisolated particles of $1 < p_T < 10\,\mathrm{GeV}$.

During the 2016–2017 data taking, a gradual shift in the timing of the inputs of the ECAL first-level trigger in the region at $|\eta| > 2.0$ caused a specific trigger inefficiency [68]. For events containing an electron (a jet) with p_T larger than ≈50 GeV (≈100 GeV), the efficiency loss is ≈10%–20%

Table 1. Baseline selection criteria used in the different final states. The electrons, muons, and τ_h are required to be well identified and isolated. The p_T and pseudorapidity ranges correspond to different sets of triggers, and different data-taking periods.

	$e\mu$	$e\tau_h$	$\mu\tau_h$	$\tau_h\tau_h$	$\mu\mu$
p_T^e (GeV)	>15/24	>25–33	—	—	—
$\lvert\eta^e\rvert$	<2.5	<2.1–2.5	—	—	—
p_T^μ (GeV)	>24/15	—	>21–29	—	>26–29/10
$\lvert\eta^\mu\rvert$	<2.4	—	<2.1–2.4	—	<2.4
$p_T^{\tau_h}$ (GeV)	—	>30–35	>30–32	>40	—
$\lvert\eta^{\tau_h}\rvert$	—	<2.1–2.3	<2.1–2.3	<2.1	—
$m_{\mu\mu}$ (GeV)	—	—	—	—	>50
OS	yes	yes	yes	yes	yes
$\lvert d_z(\ell,\ell')\rvert$ (cm)	<0.1	<0.1	<0.1	<0.1	<0.1
$\Delta R(\ell,\ell')$	>0.5	>0.5	>0.5	>0.5	>0.5
$m_T(e/\mu p_T, \vec{p}_T^{\,miss})$ (GeV)	—	<75	<75	—	—

in the region $2.5 < |\eta| < 3.0$, depending on p_T, η, and time. Correction factors were computed from data and applied to the acceptance evaluated by simulation.

5. Event selection

Events in the SR are selected in the $e\mu$, $e\tau_h$, $\mu\tau_h$, and $\tau_h\tau_h$ final states, which account for 94% of the possible final states with a pair of τ leptons. The ee and $\mu\mu$ final states have the lowest branching fractions for di$-\tau$ events and suffer from large background contributions from the photon-fusion production of electron and muon pairs, $\gamma\gamma \to ee$ and $\gamma\gamma \to \mu\mu$. Therefore, they are not considered as part of the signal. However, the $\mu\mu$ final state, which, in comparison to the ee final state, benefits from lower p_T thresholds at trigger level and higher lepton reconstruction and identification efficiencies, is used to derive corrections to:

- The pileup track density in all simulations, described in section 6.1;
- The hard scattering track multiplicity in the DY and diboson simulations, described in section 6.2;
- The elastic photon-fusion simulations to include dissociative contributions, described in section 7;
- The acoplanarity distribution in the DY simulation, described in section 8.1.

In the $e\mu$ final state, events are recorded with a combination of triggers requiring an electron and a muon, with a p_T threshold of 23 GeV for the leading lepton, and 8 (12) GeV for the subleading muon (electron). Offline, the leading (subleading) lepton is required to have $p_T > 24$ (15) GeV. The subleading lepton p_T threshold is chosen to reduce background processes with misidentified jets. In the $e\tau_h$ ($\mu\tau_h$) final states, events are recorded with single-electron (single-muon) triggers with p_T thresholds ranging between 25 and 32 (24 and 27) GeV depending on the data-taking year. Additional events with e or μp_T as low as 24 (19) GeV and $|\eta| < 2.1$ can be selected using triggers requiring also the presence of a τ_h candidate with $p_T > 20$ (27) GeV and $|\eta| < 2.1$. In these two final states, the $\tau_h p_T$ is required to be above 30 GeV offline and the background from W + jets is reduced by requiring the transverse mass m_T between the e or μp_T and $\vec{p}_T^{\,miss}$ to be less than 75 GeV. The events in the $\tau_h\tau_h$ final state are selected with triggers requiring the presence of two loosely isolated τ_h candidates with $p_T > 35$–40 GeV, depending on the data-taking year, and $|\eta| < 2.1$. The offline thresholds are $p_T > 40$ GeV and $|\eta| < 2.1$ for all the data-taking periods. A trigger requiring a single muon with $p_T > 24$–27 GeV is used to select events in the $\mu\mu$ final state. Offline, the leading (subleading) muon is required to have $p_T > 26$–29 (10) GeV and $|\eta| < 2.4$. The invariant mass of the two muons, $m_{\mu\mu}$, must be greater than 50 GeV.

In all final states, the two objects are required to be well-identified and isolated, to have opposite sign (OS) charge, to be separated from each other by $\Delta R = \sqrt{(\Delta\eta)^2 + (\Delta\phi)^2} > 0.5$, and to satisfy $|d_z(\ell,\ell')| < 0.1$ cm, where $|d_z(\ell,\ell')|$ is the difference in the longitudinal impact parameters of the two objects. In each final state, we veto events that have additional identified and isolated electrons or muons, such that one event can enter at most one final state.

The criteria listed above and summarized in table 1 constitute the baseline selection. Additional requirements are applied to define the SR or the control regions (CRs) used to derive corrections. Additional requirements increasing the signal-to-background ratio in the SR using the characteristics of the exclusive process signature are described in the following paragraphs.

The acoplanarity, defined as:

$$A = 1 - |\Delta\phi(\ell,\ell')|/\pi, \tag{7}$$

is typically small for events from the elastic photon-fusion production, for which the leptons are produced back-to-back. In the case of τ leptons, A is computed using the visible decay products, which are closely aligned with the original τ lepton before decay, especially at high p_T. In the SR, the events are required to have $A < 0.015$. This requirement has a signal efficiency ranging from 95% in the $e\mu$ final state to >99% in the $\tau_h\tau_h$ final state.

Elastic signal events are also characterized by a low track multiplicity (N_{tracks}) at the dilepton vertex. The dilepton vertex position along the z axis is calculated as the average z of

the two objects. The variable N_{tracks} is estimated by counting the number of tracks that have a z coordinate within a 0.1 cm wide window centered around the dilepton vertex, removing the tracks that were used to build the lepton candidates. The window size is chosen such that about 50% of the signal events have $N_{\text{tracks}} = 0$. This fraction is larger far from the beamspot position (z_{BS}), where the contribution from pileup tracks is less important. The SRs are defined with $N_{\text{tracks}} = 0$ or 1. About 25% of the signal events have $N_{\text{tracks}} = 1$.

A low pileup activity in the tracker, corresponding to low N_{tracks} values at the interaction vertex, impacts the identification of electrons, muons, and τ_{h} candidates, typically leading to a higher identification and isolation efficiency. Scale factors are computed to match the simulated efficiencies to the observed efficiencies for objects surrounded by a low track activity at their vertex.

6. Corrections to the simulated track multiplicity

The simulations are corrected to accurately describe N_{tracks}. We derive corrections for two sources of tracks: tracks originating from the pileup (section 6.1) and tracks originating from the hard scattering and underlying event activity (section 6.2). They are derived from the dimuon CR and applied to simulations in the SRs.

6.1. Tracks originating from pileup

While the pileup multiplicity in simulation is reweighted to match that observed in the data, the pileup track density along the z axis in simulation needs to be corrected to better describe N_{tracks} at the dilepton vertex. First, the simulations are corrected, independently for each data-taking period, such that the z_{BS} and beamspot width (σ_{BS}) distributions are similar to the observed ones. In data collected between 2016–2018, z_{BS} (σ_{BS}) is approximately in the range between -0.5 and $+1.2$ cm (3.1 and 4.2 cm). The pileup tracks are redistributed accordingly along the z axis, as explained below. Simulated events originally all have $\sigma_{\text{BS}} = 3.5\,\text{cm}$, whereas the observed σ_{BS} distribution is spread between about 3.0 and 3.8 cm. Simulated events are assigned randomly corrected beamspot properties, $z_{\text{BS}}^{\text{corr}}$ and $\sigma_{\text{BS}}^{\text{corr}}$, following the corresponding profiles in data. The z positions of pileup tracks, identified as such using generator-level information, are corrected for beamspot effects:

$$z^{\text{corr}} = z_{\text{BS}}^{\text{corr}} + \frac{\sigma_{\text{BS}}^{\text{corr}}}{\sigma_{\text{BS}}^{\text{sim}}}\left(z - z_{\text{BS}}^{\text{sim}}\right). \tag{8}$$

A residual correction to the pileup track density is derived in a $\text{Z} \to \mu\mu$ CR, defined with the selection criteria for the $\mu\mu$ final state detailed in section 5, with the additional requirement that $m_{\mu\mu}$ is within 15 GeV of the Z boson mass, m_{Z}. The track multiplicity is counted in data and in simulation in windows of 0.1 cm along the z axis, for windows centered at least 1 cm away from the reconstructed dimuon vertex, as illustrated in Figure 2. This last requirement ensures that all tracks in the windows come from pileup and not from the hard-scattering interaction. Weights are derived as functions of the pileup track multiplicity and window z position so as to match the N_{tracks} distribution of the observed events. Distributions of the number of pileup tracks, $N_{\text{tracks}}^{\text{PU}}$, are shown for the measured events, and for the uncorrected and beamspot-corrected simulations in figure 3, for windows with different z positions. About one third of the windows situated at the beamspot center do not have any pileup track. This fraction reaches about 50 (80)% one (two) beamspot width(s) away from the beamspot center. The correction to the simulated event weight is in the range 0.89–1.00 (0.93–1.16) for $N_{\text{tracks}}^{\text{PU}} = 0$ ($N_{\text{tracks}}^{\text{PU}} = 1$) over the whole z axis and data-taking periods. It is evaluated at the z position of the selected dilepton candidate.

6.2. Tracks originating from the hard scattering and underlying event activity

The only major background in the SR estimated using simulation is the DY production of a lepton pair. The number of tracks coming from the hard scattering interaction is not well described in the simulation, and corrections are derived from the same $\text{Z} \to \mu\mu$ CR, in which $m_{\mu\mu}$ is required to be within 15 GeV of m_{Z}, by comparing the number of tracks around the reconstructed dimuon vertex between data and simulation.

As shown in figure 4, the simulation is split into several components depending on the number of tracks with $p_{\text{T}} > 0.5\,\text{GeV}$ and $|\eta| < 2.5$, identified as originating from the hard scattering interaction using generator-level information, and not matched to the selected muons. The total number of reconstructed tracks, excluding the two muon tracks, is the sum of these tracks and those associated with pileup interactions: $N_{\text{tracks}} = N_{\text{tracks}}^{\text{HS}} + N_{\text{tracks}}^{\text{PU}}$. Events from the exclusive photon-fusion production of a pair of muons or W bosons, which contribute significantly only at low N_{tracks}, are estimated from simulation and subtracted.

The pileup track density is first corrected with the weights described in section 6.1, whereas the reweighting factors for each DY component with a given number of $N_{\text{tracks}}^{\text{HS}}$ is determined iteratively by matching the simulation to the observed data, starting from events with $N_{\text{tracks}} = 0$, to which only the simulated component with $N_{\text{tracks}}^{\text{HS}} = 0$ contributes. The corrections are determined separately for the different data-taking years. We checked that the requirement for $m_{\mu\mu}$ be compatible with m_{Z} introduces a bias for events with large dilepton mass, which is negligible with respect to other systematic uncertainties described in section 9. The event weight correction is as low as 0.61 ± 0.04 (0.76 ± 0.04) for $N_{\text{tracks}}^{\text{HS}} = 0$ ($N_{\text{tracks}}^{\text{HS}} = 1$). This correction is also applied to the minor diboson background with 2 leptons and 2 neutrinos in the final state, which has the same generator settings as the DY simulation.

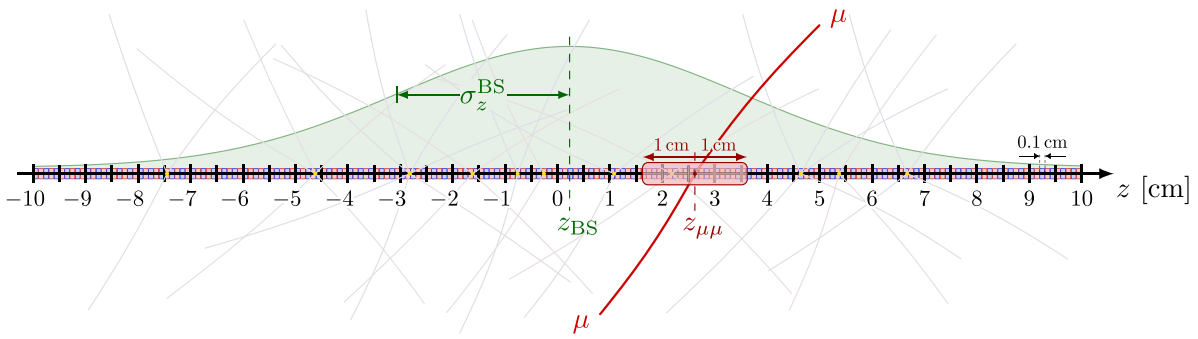

Figure 2. Schematic view of the 0.1 cm wide windows probed along the z axis to derive corrections to the pileup track density in simulation. Windows within 1 cm from the dimuon vertex, illustrated with the red box, are discarded so as not to count tracks from the hard-scattering interaction. The green curve indicates the probability distribution of z-coordinates for PU vertices in the beamspot.

7. Signal estimation

The signal is modeled using events of elastic pp scattering. The semidissociative and fully dissociative production modes are much less likely to satisfy the acoplanarity and N_{tracks} requirement, but they contribute a nonnegligible number of events to the SRs because of their larger cross sections.

The prediction from the elastic photon-fusion production is rescaled to account for the semidissociative and fully dissociative contributions. The scaling factor comes from data observed in a $\mu\mu$ CR, defined with the baseline selection summarized in table 1 and $N_{\mathrm{tracks}} = 0$ or 1 and $A < 0.015$ as additional requirements. To perform this measurement, the inclusive backgrounds, dominated by the DY production of a muon pair, are estimated together from observed events. Their $m_{\mu\mu}$ distribution is taken from observed events with $3 < N_{\mathrm{tracks}} < 7$. These thresholds ensure that the photon-fusion contributions are negligible, while preserving the $m_{\mu\mu}$ distribution. The compatibility of the $m_{\mu\mu}$ distributions in inclusive events with $N_{\mathrm{tracks}} < 2$ and $3 < N_{\mathrm{tracks}} < 7$ was verified in simulation. The $m_{\mu\mu}$ distribution is scaled so that the inclusive background normalization in the range $|m_{\mu\mu} - m_{\mathrm{Z}}| < 15\,\mathrm{GeV}$ matches the event count observed in the same range. The $\gamma\gamma \to \mu\mu$ prediction for the elastic production is then rescaled to match the difference between the experimental data and the inclusive backgrounds away from the Z peak region, as shown in figure 5.

Assuming no dependence on the dilepton mass, $m_{\ell\ell}$, the scaling factor to include the dissociative contributions is 2.70 ± 0.04 (2.71 ± 0.10) for $N_{\mathrm{tracks}} = 0$ (1), where the uncertainty is statistical only. This is compatible with the value predicted by the SuperChic generator, using the same acoplanarity requirement $A < 0.015$. The scale factor is also fitted as a linear function of $m_{\mu\mu}$, which demonstrates a better χ^2, and, in that case, is equal to $2.36 + 0.0034\ m_{\mu\mu}/\mathrm{GeV}$ ($2.38 + 0.0032\ m_{\mu\mu}/\mathrm{GeV}$) for $N_{\mathrm{tracks}} = 0$ (1). The fit probability is also better with a linear function for the predictions of the SuperChic generator, and a comparable parameterization is obtained. A linear dependency of the scaling factor with $m_{\ell\ell}$ is assumed as a nominal correction in the SRs, whereas the flat value is considered as a systematic uncertainty as detailed in section 9. Elastic events in the SR, coming from the $\gamma\gamma \to \tau\tau/\mathrm{ee}/\mu\mu/\mathrm{WW}$ simulations, are all rescaled with this correction as a function of the dilepton or diboson mass, to include semidissociative and fully dissociative contributions.

8. Background estimation

In the SR, the dominant backgrounds are the DY production of a lepton pair and processes with a jet misidentified as an electron, a muon, or a τ_{h} candidate, collectively denoted as 'jet mis-ID background'. This background is dominantly composed of W + jets and quantum chromodynamics (QCD) multijet events. The photon-fusion production of a pair of W bosons is reduced with the acoplanarity requirement, and is significant only in the eμ final state, where its expected contribution is about 4% of the exclusive di-τ production. The photon-fusion production of an electron (muon) pair is about 50 (4)% of the expected signal contribution in the eτ_{h} ($\mu\tau_{\mathrm{h}}$) final state. When there is no exclusivity requirement relying on A or N_{tracks}, the $\mathrm{t\bar{t}}$, inclusive diboson, and single top quark processes also contribute.

8.1. Drell–Yan background

The DY background is estimated using simulation. The corrections described in section 6 are applied to improve the description of $N_{\mathrm{tracks}}^{\mathrm{PU}}$ and $N_{\mathrm{tracks}}^{\mathrm{HS}}$. The acoplanarity is observed to be mismodeled by simulation in a $\mu\mu$ CR, defined with the baseline selection criteria from section 5 and further enriched in DY events by requiring $|m_{\mu\mu} - m_{\mathrm{Z}}| < 15\,\mathrm{GeV}$. An acoplanarity correction, measured in two-dimensional bins of the p_{T} of both muons, is derived in this CR by matching the simulation to the observed data. The correction is obtained by fitting the ratio of data-to-simulation with a polynomial for $A < 0.35$. For illustrative purposes, the distributions and correction obtained for all muon p_{T} bins merged together are shown in figure 6, using data collected in 2018. This acoplanarity correction is applied to simulated DY events in the SR on the basis of the generated τ lepton p_{T} before their decays.

The size of the DY simulation in the final state of a pair of electrons, muons, or τ leptons is limited, and large statistical uncertainties arise when requiring $N_{\mathrm{tracks}} = 0$ or 1. To

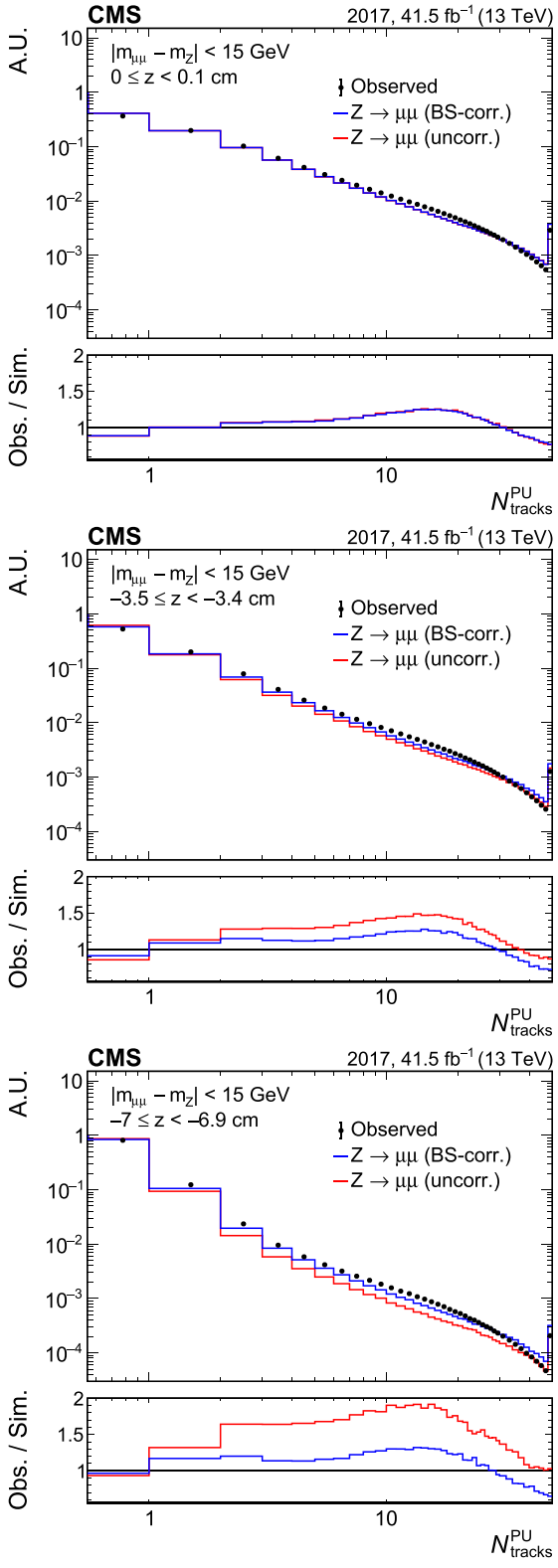

Figure 3. Distribution of N^{PU}_{tracks} in windows of 0.1 cm width along the z axis for the observed events (black), uncorrected simulation (red), and beamspot-corrected simulation (blue) for data collected in 2017. The windows shown here are located at the beamspot center (upper), and one (middle) or two (lower) beamspot widths away from the center. The ratio of beamspot-corrected simulation to observation (lower plots) is taken as a residual correction to the simulations. The last bin includes the overflow. Similar distributions and corrections are derived independently for the other data-taking periods.

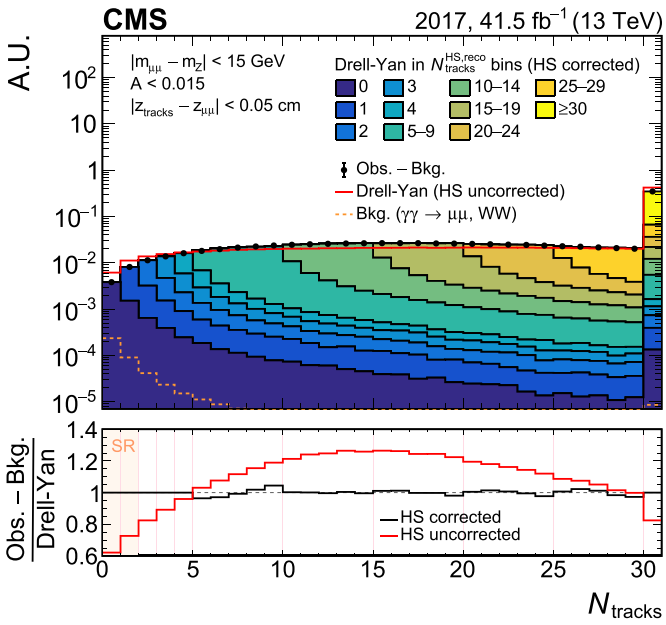

Figure 4. Distribution of the number of reconstructed tracks in a 0.1 cm wide window in the z direction, centered on the dimuon reconstructed vertex, for acoplanarity $A < 0.015$, in data collected in 2017. The DY simulation is split into several components based on the number of reconstructed tracks originating from the hard interaction. The red line shows the simulation before the correction. The black points show the observed data after subtracting the expected background contribution from the $\gamma\gamma \to \mu\mu$ and $\gamma\gamma \to$ WW processes (dashed orange line). The last bin includes the overflow. Similar distributions and corrections are derived independently for the other data-taking periods. The ratios between the observed data, from which the exclusive background contributions have been subtracted, and the DY prediction before (red) and after the corrections (black), are shown in the lower panel. The region with the selection requirement $N_{tracks} = 0$ or 1 used in the SR is highlighted with the orange shaded area in the lower panel.

reduce this effect, the DY contribution in the SR is estimated from simulated events with $N_{tracks} < 10$, which constitute about 10% of the total number of DY events. The upper bound ensures a similar event topology as in the SR, ensuring that no bias is introduced to the $m_{\tau\tau}$ distributions, as verified in simulation. The distribution derived with $N_{tracks} < 10$ is scaled to predict the DY events with $N_{tracks} = 0$ or 1. The scale factors are derived in the eμ final state with a simulation with a large number of $Z/\gamma* \to \tau\tau$ events with only leptonic τ decays. All the corrections described in section 6 are applied to predict the DY yield in the eμ final state with $N_{tracks} = 0$, 1, or <10. The scale factors are equal to $(2.48 \pm 0.05)\%$ and $(5.10 \pm 0.07)\%$, for $N_{tracks} = 0$ and 1, respectively. In the eμ final state, the large simulation with leptonic τ decays is used instead of reweighting events with $N_{tracks} < 10$.

8.2. Backgrounds with misidentified jets in the eτ_h and $\mu\tau_h$ final states

The mis-ID background with a jet misidentified as a τ_h candidate is estimated from the experiment. In the eτ_h and $\mu\tau_h$ final

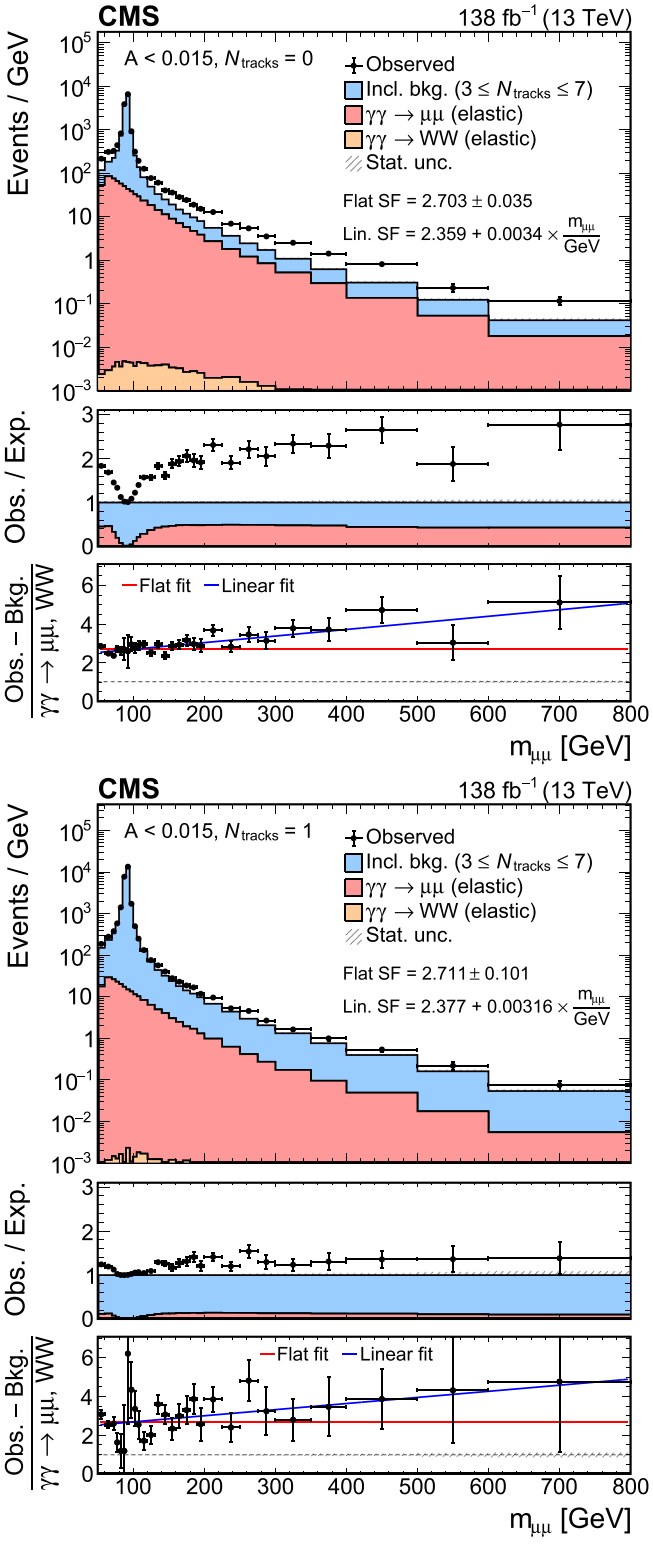

Figure 5. Measurement of the scale factor for the elastic exclusive signal in $\mu\mu$ events for $N_{\text{tracks}} = 0$ (upper) or 1 (lower), and $A < 0.015$. The shape of the inclusive background (blue) is estimated from the observed data in the $3 \leqslant N_{\text{tracks}} \leqslant 7$ sideband, and rescaled to fit the observed data in $75 < m_{\mu\mu} < 105\,\text{GeV}$. The scale factor is fitted in the lower ratio panel with constant (red) and linear (blue) functions. The vertical error bars indicate the statistical uncertainty in the number of observed events.

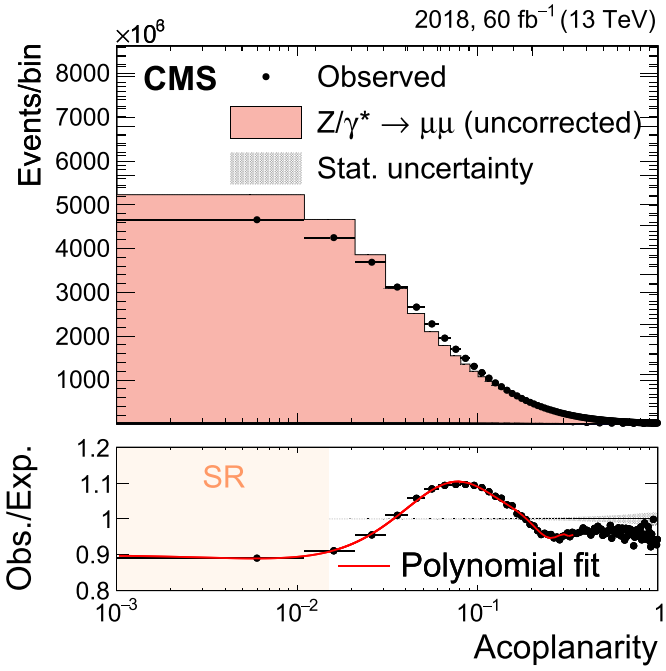

Figure 6. Acoplanarity distribution for the observed events and in DY simulation before correction, in the 2018 data-taking period. The background prediction is normalized to match the observed yield and only the statistical uncertainty is shown. The data-to-simulation ratio is fitted with a polynomial to obtain the correction. The selection criterion $A < 0.015$ used in the SR is highlighted with the orange shaded area in the lower panel.

states, the dominant processes contributing to the mis-ID background are W + jets and QCD multijet events. The jet misidentification factors (MFs) depend on the process because of different topologies and jet flavors, and they are therefore measured in two different CRs. A CR enriched in W + jets events is built by requiring $m_{\text{T}} > 75\,\text{GeV}$, whereas a QCD-enriched CR is obtained by requiring the two objects to have same-sign (SS) charge. There is no requirement on N_{tracks} at this stage. In these CRs, the MFs are measured for each data-taking period, separately for each τ_{h} DM ($\text{DM}^{\tau_{\text{h}}}$), by taking the ratio of events in which the τ_{h} candidate passes the SR τ_{h} identification criteria, to events in which the τ_{h} candidate fails these criteria but passes looser ones. Events where the τ_{h} candidate is genuine or corresponds to a misidentified electron or muon are evaluated using simulation and subtracted from the CR. The MFs are fitted as functions of the $\tau_{\text{h}} p_{\text{T}}$ and range from about 0.03 for the $\text{h}^{\pm}\text{h}^{\mp}\text{h}^{\pm} + \pi^0$(s) DM, to about 0.40 for the $\text{h}^{\pm}$ DM. The MFs are measured in events recorded with single-electron or -muon triggers. The triggers that select τ_{h} candidates in addition to electrons or muons, called 'cross-triggers', apply loose isolation requirements to the τ_{h} candidates at trigger level, such that the MFs are modified. The MF measured in events selected with cross-triggers is measured to be 1.7 times higher than the average MF in events selected with single-lepton triggers, and this factor is applied as a multiplicative correction to the MFs for events recorded with a cross-trigger.

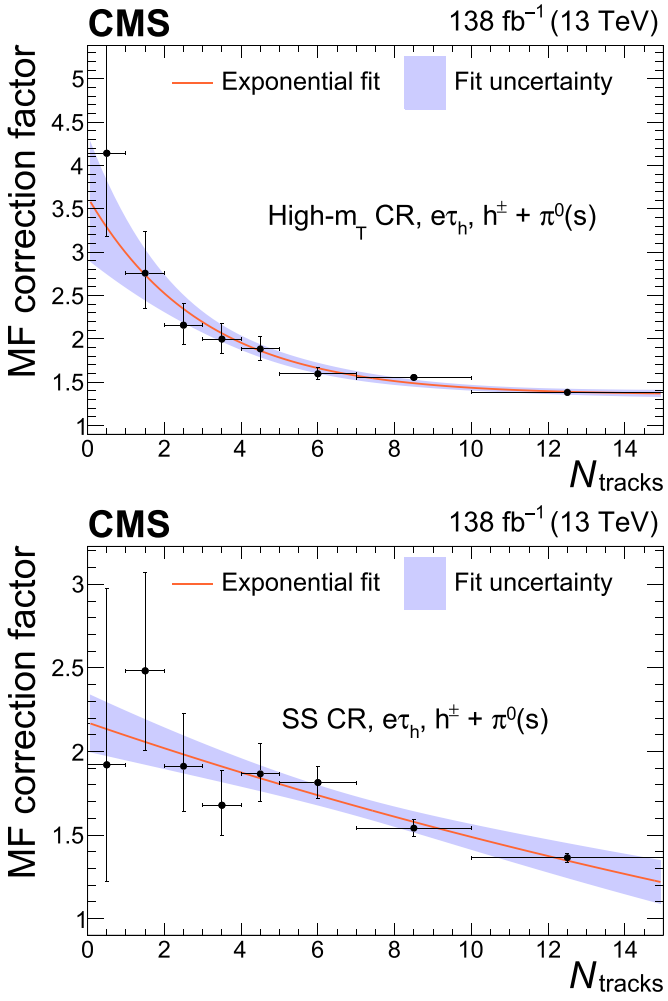

Figure 7. Multiplicative N_{tracks}-dependent corrections to the τ_h MFs, $\omega(N_{\text{tracks}}, \text{DM}^{\tau_h})$, in the $e\tau_h$ final state, in the high-m_T (upper) and SS (lower) CRs, for the $h^{\pm} + \pi^0$(s) DM. The purple shaded area corresponds to the fit uncertainty. The vertical error bars indicate the statistical uncertainty in the MF correction factors measured in individual N_{tracks} ranges.

The track activity around the di-τ system impacts the calculation of the τ_h isolation, which enters the τ_h identification discriminator, such that the MFs are expected to depend on N_{tracks}. For each τ_h DM, the MFs determined for given ranges of N_{tracks} are divided by the average MF measured inclusively in N_{tracks} to obtain a multiplicative N_{tracks}-dependent correction, $\omega(N_{\text{tracks}}, \text{DM}^{\tau_h})$, to the p_T- and decay-mode-dependent MFs determined previously. The corrected MFs can then be written, for each CR, as:

$$\begin{aligned}&\text{MF}^{\text{corr}}\left(p_T{}^{\tau_h}, \text{DM}^{\tau_h}, N_{\text{tracks}}\right)\\ &\quad = \text{MF}\left(p_T{}^{\tau_h}, \text{DM}^{\tau_h}\right)\omega\left(N_{\text{tracks}}, \text{DM}^{\tau_h}\right).\end{aligned} \tag{9}$$

The $\omega(N_{\text{tracks}}, \text{DM}^{\tau_h})$ corrections are measured for the combination of the different data-taking years. Because statistical uncertainties are large at low N_{tracks}, $\omega(N_{\text{tracks}}, \text{DM}^{\tau_h})$ is fitted with an exponential function for N_{tracks} less than 10 or 15, depending on the τ_h DM, as shown in figure 7 for the $h^{\pm} + \pi^0$(s) DM in the $e\tau_h$ final state.

The total MF, MF^{tot}, is computed as a weighted average of the MFs determined in the high-m_T and SS CRs, according to the expected relative fraction of W + jets and QCD multijet events:

$$\text{MF}^{\text{tot}} = x^{\text{QCD}}\text{MF}^{\text{corr}}_{\text{SS}} + \left(1 - x^{\text{QCD}}\right)\text{MF}^{\text{corr}}_{\text{high-m}_T}, \tag{10}$$

where $x^{\text{QCD}} = N^{\text{QCD}}/(N^{\text{QCD}} + N^{\text{W}})$. The number of W + jets events passing the baseline selection, N^{W}, is determined from simulations, whereas the same quantity for QCD multijet events, N^{QCD}, is taken as the difference between data and simulated predictions for other processes in the SS CR.

To estimate the mis-ID background in the SR in the $e\tau_h$ and $\mu\tau_h$ final states, events passing the SR selection with the exception that the τ_h candidate fails the τ_h nominal identification but passes looser criteria, are reweighted with MF^{tot}. Contributions from events with real τ_h, electrons, or muons are estimated from simulation and subtracted from the anti-isolated region.

8.3. Backgrounds with misidentified jets in the $\tau_h\tau_h$ final state

In the $\tau_h\tau_h$ final state, the mis-ID background is mostly composed of QCD multijet events and the MFs are determined in a single CR where the τ_h candidates have SS charge. The MFs for the leading (subleading) τ_h are measured in events in which the subleading (leading) τ_h passes or fails the tight identification criteria. They are in the range 0.05–0.38 depending on the τ_h DM.

The N_{tracks}-dependent correction is derived in a similar way as in the $e\tau_h$ and $\mu\tau_h$ final states, and is between 1.8 and 2.3 for events with $N_{\text{tracks}} = 0$. In the $\tau_h\tau_h$ state, the number of events selected at low N_{tracks} is larger because of the inversion of the isolation of both τ_h candidates, and contributions from exclusive dijet production become significant in the lowest N_{tracks} bins, such that no fit is performed to the $\omega(N_{\text{tracks}}, \text{DM}^{\tau_h})$ distributions. The values for $N_{\text{tracks}} = 0, 1$ are used without constraints events with $N_{\text{tracks}} > 1$.

In the SR, events in which the leading (subleading) τ_h is a misidentified jet are estimated by scaling by the MFs events where the leading (subleading) τ_h is anti-isolated and the subleading (leading) τ_h is isolated. These contributions include events where both the leading and subleading τ_h candidates are misidentified jets. To remove the double counting, events with two misidentified jets are estimated by scaling events where the two τ_h candidates are anti-isolated with the product of the MFs for each object, and are subtracted.

8.4. Backgrounds with misidentified jets in the $e\mu$ final state

In the $e\mu$ final state, the mis-ID background with a jet misidentified as an electron or a muon, dominantly composed of W + jets and QCD multijet events, is estimated from events where the electron and muon have SS charge. Events passing the SR selection with the exception that the electron and muon have SS charge are reweighted with a two-dimensional scale factor dependent on the electron and muon p_T. This factor is measured by taking the ratio of OS-to-SS events where the

muon isolation is inverted, subtracting nonjet contributions estimated from simulation. It is in the range 1.4–2.1, depending on the lepton p_T.

A bias is introduced by the inversion of the muon isolation, which modifies the background composition, and a correction to the scale factor is measured by taking the ratio of the scale factors measured in events where the electron identification is inverted, and the muon isolation is inverted or not. The correction ranges between 1.0 and 2.7 depending on the lepton p_T.

A multiplicative correction for the dependency of the scale factor on N_{tracks} is measured by fitting the ratio of the scale factors in exclusive ranges of N_{tracks} over the average inclusive scale factor. At $N_{tracks} = 0$, the correction is about 0.89 ± 0.07, where the uncertainty is mostly from statistical origin.

Although the normalization of the jet mis-ID background is estimated with the procedure described above, its m_{vis} distribution is taken from SS data events with $N_{tracks} < 10$, from which backgrounds other than the jet mis-ID component are subtracted using their simulated expectations. This method reduces statistical fluctuations in the m_{vis} templates.

8.5. Other backgrounds

Minor contributions from diboson events to the SR, mostly WW events, are estimated from simulation. The exclusive $\gamma\gamma \to WW$, $\gamma\gamma \to ee$, and $\gamma\gamma \to \mu\mu$ events, which contribute mostly to the $e\mu$, $e\tau_h$, and $\mu\tau_h$ final states, respectively, are estimated from the elastic production simulation and rescaled with the same correction as the signal samples to include the dissociative components.

The agreement between data and predictions is checked in events passing the selection without the N_{tracks} and acoplanarity requirements. The single top quark, $t\bar{t}$, and Higgs boson processes, which do not contribute to the SR with $N_{tracks} < 2$, are included using their prediction from simulation.

9. Systematic uncertainties

Systematic uncertainties are considered as nuisance parameters in the statistical procedure to extract the signal significance, the signal strength μ, and constraints on a_τ and d_τ. They are treated with either Gaussian (shape uncertainties) or log-normal (normalization uncertainties) function priors included in the likelihood function. The signal strength μ is defined as the ratio between the observed cross section of the $\gamma\gamma \to \tau\tau$ process to the theoretical cross section predicted by the GAMMA-UPC generator for the elastic production component corrected by the multiplicative experimental scaling to include dissociative contributions.

The integrated luminosities for the 2016, 2017, and 2018 data-taking years have 1.2%–2.5% individual uncertainties [69–71], whereas the overall uncertainty for the 2016–2018 period is 1.6%. The uncertainty in the DY (diboson production) theoretical cross section is 2 (5)% [72].

The uncertainties in the electron and muon identification, isolation, and triggering efficiencies are up to 2% per object. Uncertainties related to the τ_h trigger efficiency depend on DM^{τ_h} and are up to 5%. Several uncertainties, stemming from statistical and systematic sources in the measurement, affect the τ_h identification, with different correlations across data-taking years and various dependencies on the decay mode and p_T of the τ_h candidate. This uncertainty is up to 5% in the p_T range considered in this analysis, and propagates directly to the measured signal strength. Electrons and muons misidentified as τ_h candidates, coming mostly from the $Z/\gamma* \to ee$ and $Z/\gamma* \to \mu\mu$ processes, respectively, have normalization uncertainties on the order of 10%. The uncertainty in the τ_h energy scale is up to 1.2%, whereas electrons (muons) misidentified as τ_h have energy scale uncertainties up to 5 (1)%. Multiplicative corrections to the identification and isolation scale factors to account for the low-N_{tracks} environment are derived for τ_h candidates and electrons, as well as electrons and muons misidentified as τ_h candidates. Scale factors for muons do not need to be adjusted for the low-N_{tracks} environment. The related uncertainties are 2.1% and 2.0% for τ_h candidates and electrons, and 22% and 15% for electrons and muons misidentified as τ_h candidates, respectively.

The uncertainty in the N_{tracks}^{PU} correction amounts to 2%, which covers the effects of the beamspot width and position correction. The uncertainty in the N_{tracks}^{HS} correction is taken to have the same magnitude as the relative fraction of $\gamma\gamma \to \mu\mu/WW$ events in the CR where the correction is derived, and it amounts to 6.5 (1.5)% in the $N_{tracks} = 0$ (1) category. The statistical uncertainty in the correction is negligible with respect to this systematic component. This uncertainty contributes a 7% effect in the measured signal strength as shown in figure 8(second line) and is among the leading systematic uncertainties in this analysis.

The correction to the acoplanarity distribution in simulated DY events leads to a 5% normalization uncertainty, arising from the finite granularity used to bin the correction as a function of the p_T of the two leptons. An uncertainty of 2.0 (1.4)% is associated with the estimation of the DY events in the SR with $N_{tracks} = 0$ (1) from simulated events with $N_{tracks} < 10$. Uncertainties arising from the renormalization and factorization scales, as well as from the PDF set, are also taken into account for the DY simulation, after propagation to the acoplanarity correction.

The uncertainty in the predictions of the jet mis-ID background in final states with τ_h candidates comes from several sources:

- Statistical uncertainty in the inclusive MFs, growing linearly to 50% for $p_T^{\tau_h} = 300\,GeV$, independently for each DM and data-taking year;
- Statistical uncertainty in the N_{tracks} correction, amounting to 18 (16, 6)% in the $e\tau_h$ ($\mu\tau_h$, $\tau_h\tau_h$) SRs;
- Systematic uncertainty in the inclusive MFs, coming from the inversion of selection requirements to define the CRs, reaching up to 10%;
- Systematic uncertainty in the calculation of the relative fraction of W + jets and QCD multijet events in the $e\tau_h$ and $\mu\tau_h$ SRs, leading to a 9% normalization effect;

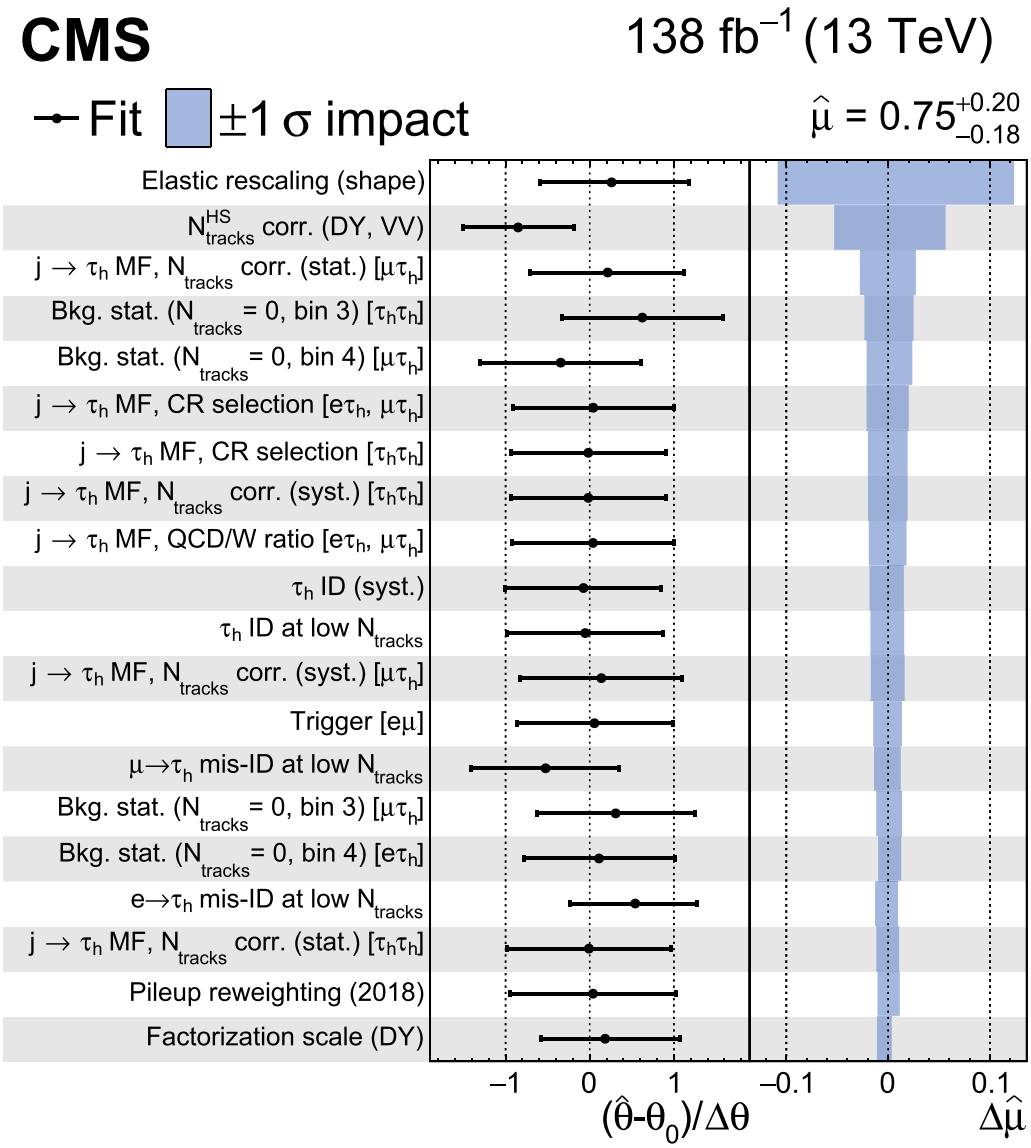

Figure 8. Postfit values of the nuisance parameters (black markers), shown as the difference of their best-fit values, $\hat{\theta}$, and prefit values, θ_0, relative to the prefit uncertainties $\Delta\theta$. The horizontal error bars indicate the uncertainties in these measured postfit values. The impact $\Delta\hat{\mu}$ of the nuisance parameter on the signal strength is computed as the difference of the nominal best fit value of μ and the best fit value obtained when fixing the nuisance parameter under scrutiny to its best fit value $\hat{\theta}$ plus/minus its postfit uncertainty (blue shaded area). The nuisance parameters are ordered by their impact, and only the 20 highest ranked parameters are shown.

- Systematic uncertainty in the N_{tracks} correction, arising from the choice of the fit function and fit range, with an effect up to 10% for $N_{\text{tracks}} = 0$.

Statistical uncertainties in the OS-to-SS scaling factor used to evaluate the mis-ID background in the eμ final state are included, independently for each bin in the electron and muon p_{T} where the measurement is performed. A systematic uncertainty of 10% is added to cover for a potential difference in the background composition in the SR and CR. The extrapolation of the scaling factor to $N_{\text{tracks}} = 0$ has a total uncertainty of 8%, arising from the choice of the fit function and from the limited number of events in the measurement.

Most theoretical and experimental uncertainties cancel when renormalizing the signal prediction using the scaling factor derived from the $\mu\mu$ CR for the $\gamma\gamma \to \mu\mu$ process. The uncertainty in the scaling factor is composed of a normalization component of statistical origin, amounting to 1.3 (3.7)% for $N_{\text{tracks}} = 0$ (1), and a component with a shape dependence on $m_{\tau\tau}$. For the latter component, we consider as a 1 standard deviation (s.d.) effect the hypothesis that the scale factor does not depend on $m_{\ell\ell}$, and is symmetrized with respect to the nominal hypothesis of a linear dependence with $m_{\ell\ell}$. This $m_{\tau\tau}$-dependent uncertainty is the leading uncertainty in the measurement of the $\gamma\gamma \to \tau\tau$ process, as shown in figure 8(first line), and contributes a 16% uncertainty to the measured signal strength. Modifying the N_{tracks} range used to extract the

Table 2. Summary of the systematic uncertainties considered in the analysis. The sources of the uncertainties, the processes they affect, and their magnitudes are indicated.

Uncertainty	Process	Magnitude
Luminosity	All simulations	1.6%
DY cross section	DY	2%
Inclusive diboson cross section	WW, WZ, ZZ	5%
e ID, iso, trigger	All simulations	up to 2%
e ID low-N_{tracks} correction	All simulations	1%
μ ID, iso, trigger	All simulations	<2%
τ_h ID	All simulations	1%–5%
τ_h trigger	All simulations	up to 5%
$e \to \tau_h$ mis-ID	$Z/\gamma* \to ee$ and $\gamma\gamma \to ee$	<10%
$\mu \to \tau_h$ ID	$Z/\gamma* \to \mu\mu$ and $\gamma\gamma \to \mu\mu$	<10%
τ_h energy scale	All simulations	<1.2%
$e \to \tau_h$ energy scale	$Z/\gamma* \to ee$ and $\gamma\gamma \to ee$	<5%
$\mu \to \tau_h$ energy scale	$Z/\gamma* \to \mu\mu$ and $\gamma\gamma \to \mu\mu$	<1%
τ_h ID low-N_{tracks} correction	All simulations	2.1%
e ID low-N_{tracks} correction	All simulations	2.0%
$e \to \tau_h$ ID low-N_{tracks} correction	$Z/\gamma* \to ee$ and $\gamma\gamma \to ee$	22%
$\mu \to \tau_h$ ID low-N_{tracks} correction	$Z/\gamma* \to \mu\mu$ and $\gamma\gamma \to \mu\mu$	15%
$N_{\text{tracks}}^{\text{PU}}$ reweighting	All simulations	2%
$N_{\text{tracks}}^{\text{HS}}$ reweighting	DY and inclusive VV	1.5%–6.5%
Acoplanarity correction	DY	5%
DY extrapolation from $N_{\text{tracks}} < 10$	DY simulation	1.4%–2.0%
μ_R, μ_f	DY simulation	Shape
PDF	DY simulation	Shape
jet$\to \tau_h$ MF, extrapolation with $p_T^{\tau_h}$	jet$\to \tau_h$ mis-ID bkg.	<50%
jet$\to \tau_h$ MF, N_{tracks} extrapolation (stat.)	jet$\to \tau_h$ mis-ID bkg.	6%–18%
jet$\to \tau_h$ MF, inversion of CR selection	jet$\to \tau_h$ mis-ID bkg.	<10%
jet$\to \tau_h$ MF, x^{QCD} fraction	jet$\to \tau_h$ mis-ID bkg.	9%
jet$\to \tau_h$ MF, N_{tracks} extrapolation (syst.)	jet$\to \tau_h$ mis-ID bkg.	<10%
jet$\to e/\mu$ OS-to-SS (stat.)	jet$\to e/\mu$ mis-ID bkg.	<20%
jet$\to e/\mu$ OS-to-SS (syst.)	jet$\to e/\mu$ mis-ID bkg.	10%
jet$\to e/\mu$ OS-to-SS N_{tracks} extrapolation	jet$\to e/\mu$ mis-ID bkg.	8%
Elastic rescaling (stat.)	$\gamma\gamma \to \tau\tau/\mu\mu/ee, WW$	1.3%–3.7%
Elastic rescaling (syst., shape)	$\gamma\gamma \to \tau\tau/\mu\mu/ee, WW$	Mass-dependent
Limited statistics	All processes	Bin-dependent
Pileup reweighting	All simulations	Event-dependent

inclusive processes in the scale factor measurement has a much smaller effect and the corresponding uncertainty is neglected. These uncertainties are also considered for the photon-fusion WW, ee, and $\mu\mu$ production.

Statistical uncertainties in the number of simulated background events in the SR or observed event yields in the CRs used to derive the jet mis-ID background are considered in all bins of the distributions using the approach from [73]. The systematic uncertainty in the pileup modeling is included by varying by $\pm 4.6\%$ the total inelastic cross section used to calculate simulated pileup distributions [74].

The impacts of the leading systematic uncertainties in the measurement of the signal strength, which is described in section 10.1, are shown in figure 8. All the systematic uncertainties are summarized in table 2.

10. Results

The significance of the $\gamma\gamma \to \tau\tau$ process, as well as the constraints on a_τ and d_τ, are extracted with a binned maximum likelihood fit from the m_{vis} distributions in the four final states and two N_{tracks} bins, shown in figures 9 and 10. Since the di-τ system is produced centrally for the signal in the fiducial region, m_{vis} is strongly correlated with the τ lepton p_T, and similarly sensitive constraints on a_τ and d_τ could be set using p_T distributions. The CMS statistical analysis and combination tool COMBINE is used [75]. The last bins include events up to $m_{\text{vis}} = 500\,\text{GeV}$, and events at higher m_{vis} are discarded to ensure a sufficient difference with the Λ scale used in the BSM interpretation. This upper threshold removes SM signal events at the percent level. The lower m_{vis} thresholds depend on the final state because of different p_T thresholds arising

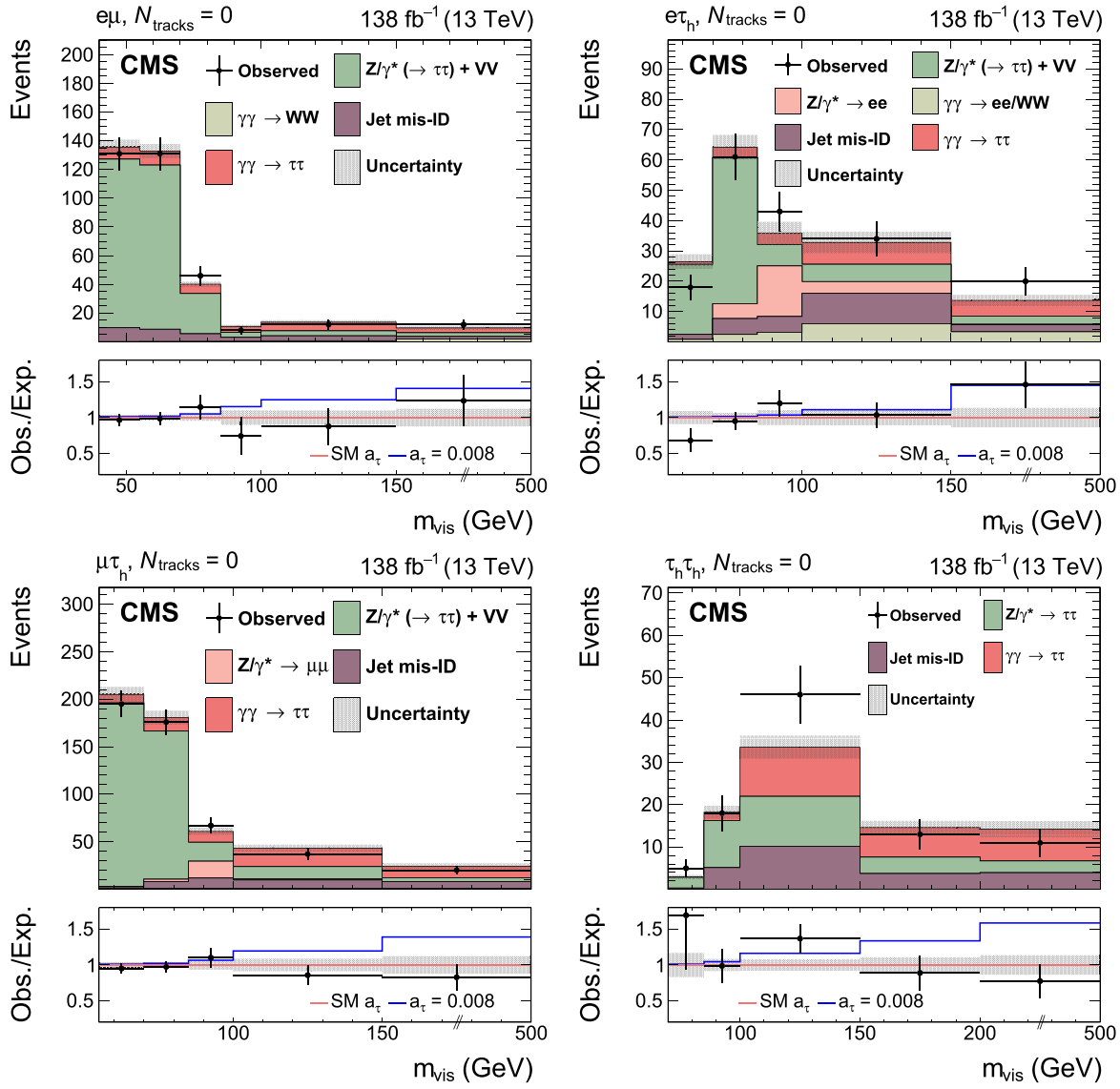

Figure 9. Observed and predicted m_{vis} distributions in the eμ (upper left), eτ_h (upper right), $\mu\tau_h$ (lower left), and $\tau_h\tau_h$ (lower right) final states for events with $N_{tracks} = 0$, the lower panels showing the observed/expected ratio. The observed data and their associated Poissonian statistical uncertainty are shown with black markers with vertical error bars. The minor inclusive diboson background contribution is drawn together with the DY background in the eμ, eτ_h, and $\mu\tau_h$ final states. The predicted background distributions correspond to the result of the global fit. The signal distribution is normalized to its best fit signal strength. The uncertainty band accounts for all sources of background and signal uncertainty, systematic as well as statistical, after the global fit. In the fit, a_τ and d_τ are fixed to their SM values. The ratio of the total predictions for an illustrative value of $a_\tau = 0.008$ to those with SM electromagnetic couplings is shown with a blue line in the lower panel of each plot.

from trigger requirements. The sources of systematic uncertainties described in section 9 are included in the statistical procedure as nuisance parameters. The number of data events in the $N_{tracks} = 0$ SRs, with the additional requirement that m_{vis} is greater than 100 GeV to reduce the DY background contribution, is compared in table 3 to the background and signal yields in the different final states.

10.1. Observation of $\gamma\gamma \to \tau\tau$

The observed (expected) significance, calculated with the asymptotic approximation [76] using COMBINE, is 5.3 (6.5) s.d. for the exclusive $\gamma\gamma \to \tau\tau$ process. This constitutes the first observation of this process in pp collisions. The corresponding observed (expected) significances per final state are 2.3, 3.0, 2.1, and 3.4 (3.2, 2.1, 3.9, and 3.9) s.d. in the eμ, eτ_h, $\mu\tau_h$, and $\tau_h\tau_h$ final states, respectively. We measure a best fit signal strength of $\hat{\mu} = 0.75^{+0.21}_{-0.18}$, where the systematic uncertainty dominates over the statistical uncertainty ($\hat{\mu} = 0.75^{+0.17}_{-0.14}(\text{syst}) \pm 0.11(\text{stat})$). This corresponds to a 1.2 s.d. with respect to the theoretical cross section predicted by the GAMMA-UPC generator for the elastic production component corrected by the multiplicative experimental scaling to include dissociative contributions.

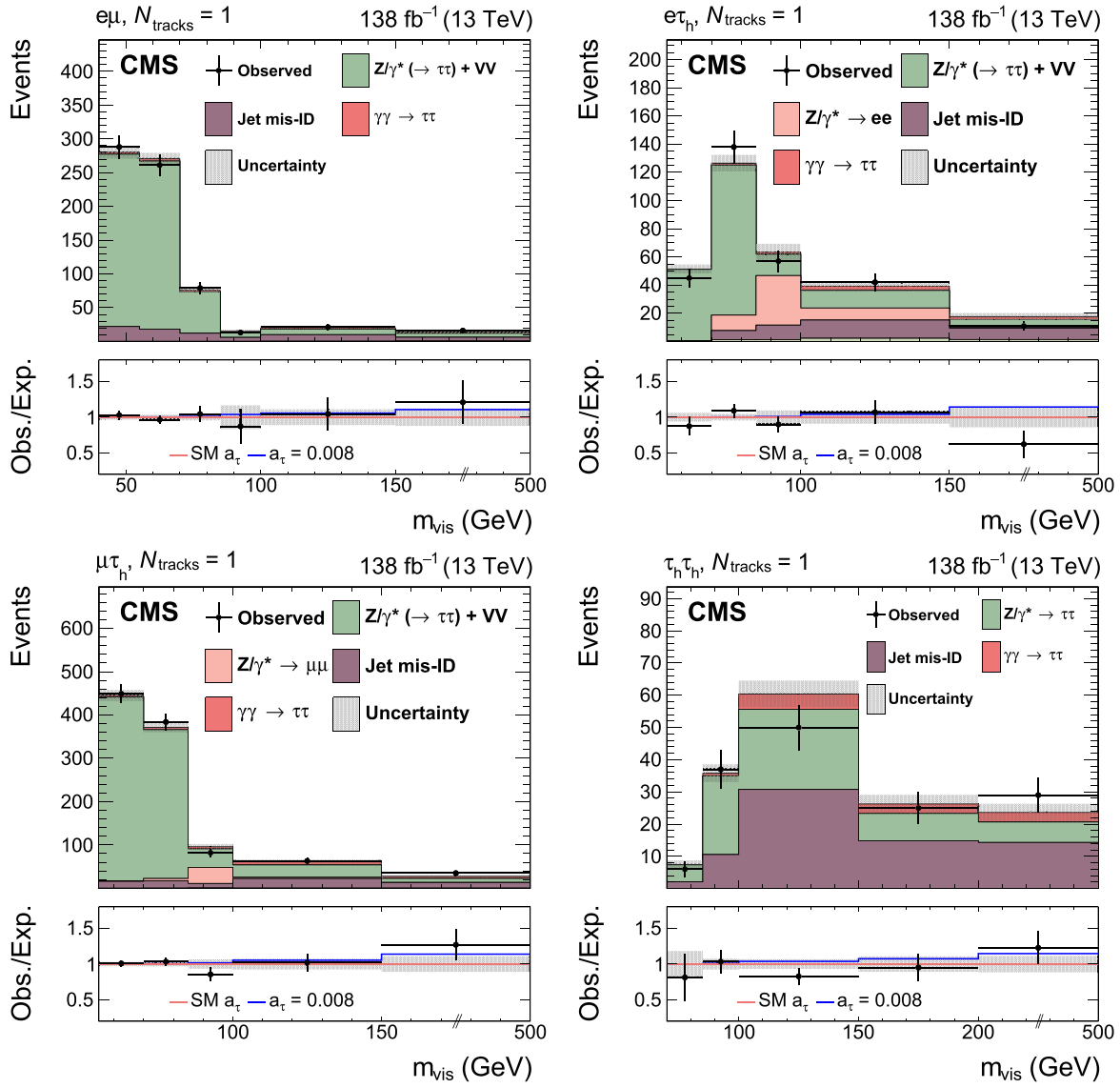

Figure 10. Observed and predicted m_{vis} distributions in the eμ (upper left), eτ_h (upper right), $\mu\tau_h$ (lower left), and $\tau_h\tau_h$ (lower right) final states for events with $N_{tracks} = 1$. The description of the histograms is the same as in figure 9.

Table 3. Observed and predicted event yields per final state in the signal-enriched phase space with $m_{vis} > 100\,GeV$ and $N_{tracks} = 0$. The signal and background yields are the result of the global fit including all sources of uncertainties.

Process	eμ	eτ_h	$\mu\tau_h$	$\tau_h\tau_h$
$Z/\gamma^* \to \tau\tau$	3.2 ± 0.5	8.2 ± 1.2	16.6 ± 2.9	18.4 ± 3.1
$Z/\gamma^* \to ee/\mu\mu$	—	4.0 ± 1.2	1.2 ± 0.6	—
Jet mis-ID	5.2 ± 0.8	12.3 ± 2.9	15.9 ± 3.6	17.9 ± 2.8
Inclusive VV	2.8 ± 0.3	0.23 ± 0.02	0.33 ± 0.3	—
$\gamma\gamma \to ee/\mu\mu$	—	9.2 ± 2.3	1.3 ± 0.2	—
$\gamma\gamma \to WW$	2.7 ± 0.6	0.16 ± 0.04	0.4 ± 0.1	—
Total bkg.	13.9 ± 1.3	34.1 ± 4.8	35.7 ± 4.4	36.3 ± 4.2
Signal	9.5 ± 2.0	12.4 ± 2.6	31.6 ± 6.7	26.1 ± 5.8
Total	23.4 ± 1.7	46.5 ± 5.4	67.3 ± 6.8	62.4 ± 6.2
Observed	24	54	57	70

The N_{tracks} distribution for events with $N_{tracks} < 10$ is shown for the combination of final states in figure 11 for events with $A < 0.015$, as in the SR, and $m_{vis} > 100\,GeV$, so as to reduce the DY background contribution. The signal contribution is visible as an excess of events over the inclusive background in the first bins, whereas the

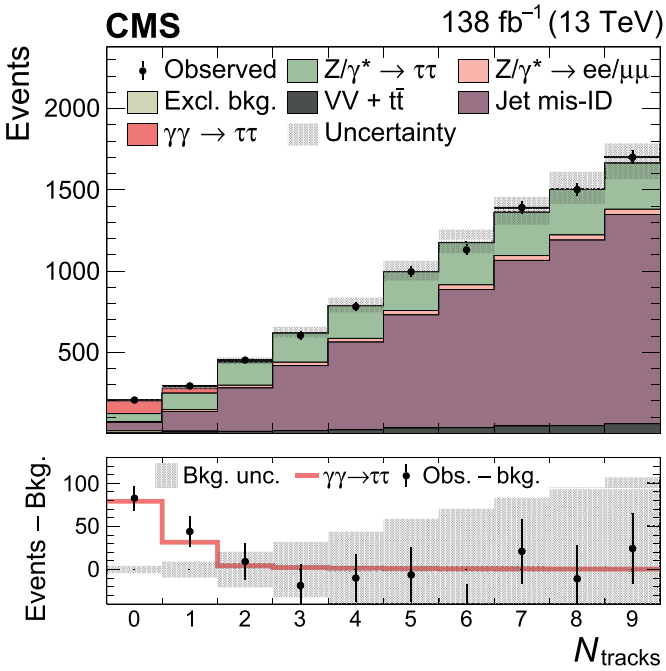

Figure 11. Observed and predicted N_{tracks} distributions for events passing the SR selection but with the relaxed requirement $N_{\text{tracks}} < 10$ and the additional requirement $m_{\text{vis}} > 100\,\text{GeV}$, combining the e$\mu$, e$\tau_h$, $\mu\tau_h$, and $\tau_h\tau_h$ final states together. The acoplanarity requirement $A < 0.015$ is applied. The observed data and their associated Poissonian statistical uncertainty are shown with black markers with vertical error bars. The inclusive diboson background contribution is drawn together with that of the $t\bar{t}$ process. The predicted distributions are adjusted to the result of the global fit performed with the m_{vis} distributions in the SRs, and the signal distribution is normalized to its best fit signal strength. The lower panel shows the difference between the observed events and the backgrounds, as well as the signal contribution. Systematic uncertainties are assumed to be uncorrelated between final states to draw the uncertainty band.

agreement between prediction and observation in the other bins demonstrates a good background modeling, more specifically in terms of N_{tracks} corrections to the simulations and MFs used to predict the background with misidentified jets.

The fiducial cross section of the $\gamma\gamma \to \tau\tau$ process is measured using only the SR with $N_{\text{tracks}} = 0$, because it is not possible to extract the origin of the track in the SR with $N_{\text{tracks}} = 1$ given the procedure used to estimate dissociative contributions. In this measurement, signal events not belonging to the fiducial region but entering the reconstruction-level categories are constrained to their expected normalizations and distributions, within uncertainties. The cross section of the $\gamma\gamma \to \tau\tau$ process is measured in a fiducial phase space defined to be as close as possible to the reconstructed event selection. All variables used in the definition of the fiducial region are calculated at the generator level after parton showering and hadronization, and the lepton momentum includes the momenta of photons radiated within a cone of $\Delta R < 0.1$ centered on the lepton. The visible τ lepton decay products at the generator level are required to have an acoplanarity $A < 0.015$ and an invariant mass less than 500 GeV. The di-τ invariant mass, including the neutrinos, is required to be greater than 50 GeV. There must not be any stable charged particle with $p_T > 0.5\,\text{GeV}$ and $|\eta| < 2.5$ outside of the τ lepton decay products. The other requirements depend on the final state. In the eμ final state, the leading lepton must satisfy $p_T > 24\,\text{GeV}$ whereas the requirement for the subleading lepton is $p_T > 15\,\text{GeV}$. The electron (muon) must have $|\eta| < 2.5$ (2.4). In the eτ_h ($\mu\tau_h$) final state, the electron (muon) is required to have $p_T > 25\,\text{GeV}$ and $|\eta| < 2.5$ ($p_T > 21\,\text{GeV}$ and $|\eta| < 2.4$), whereas the visible τ_h must have $p_T > 30\,\text{GeV}$ and $|\eta| < 2.3$. In addition, the transverse mass $m_T(e/\mu, \vec{p}_T^{\,\text{miss}})$ must be less than 75 GeV. In the $\tau_h\tau_h$ final state, the p_T sum of the visible τ_h decay products at the generator level must be greater than 40 GeV for both τ_h candidates, and the visible momentum vectors must lie within $|\eta| < 2.3$. Other di-τ final states are considered to be outside of the fiducial region. The definition of the fiducial region is summarized in table 4. Using the SRs with $N_{\text{tracks}} = 0$, the fiducial

Table 4. Selection criteria to define the fiducial cross section. Events where the two τ leptons decay both to electrons or to muons, with neutrinos, are considered to be outside the fiducial region. All requirements are applied using generator-level quantities, as detailed in the text.

	eμ	eτ_h	$\mu\tau_h$	$\tau_h\tau_h$
p_T^e (GeV)	>15/24	>25	—	—
$\lvert\eta^e\rvert$	<2.5	<2.5	—	—
p_T^μ (GeV)	>24/15	—	>21	—
$\lvert\eta^\mu\rvert$	<2.4	—	<2.4	—
$p_T^{\tau_h}$ (GeV)	—	>30	>30	>40
$\lvert\eta^{\tau_h}\rvert$	—	<2.3	<2.3	<2.3
$\Delta R(\ell, \ell')$	>0.5	>0.5	>0.5	>0.5
$m_T(e/\mu, \vec{p}_T^{\,\text{miss}})$ (GeV)	—	<75	<75	—
A	<0.015	<0.015	<0.015	<0.015
m_{vis} (GeV)	<500	<500	<500	<500
N_{tracks}	0	0	0	0

cross section is measured to be $\sigma^{\text{fid}}_{\text{obs}} = 12.4^{+3.8}_{-3.1}$ fb. This can be compared with the prediction from the GAMMA-UPC generator for the elastic production component of the signal, rescaled by the correction based on control samples in the measured events to include dissociative contributions: $\sigma^{\text{fid}}_{\text{pred}} = 16.5 \pm 1.5$ fb, where the uncertainty is dominated by the data-driven correction.

10.2. Constraints on the anomalous electromagnetic moments of the τ lepton

Constraints on a_τ and d_τ are set independently by performing a binned likelihood scan with a_τ and d_τ as single parameters of interest. Unlike in section 10.1, a_τ and d_τ are allowed to float, one at a time, whereas the normalization and m_{vis} distribution of the $\gamma\gamma \to \tau\tau$ process under the SM hypothesis is constrained to its predicted value, estimated from the elastic production simulation [38] and weighted with the scale factor from the $\mu\mu$ CR to include dissociative contributions. Varying a_τ and d_τ from their SM values modifies both the normalization of the signal process and its m_{vis} distribution. In particular, the number of predicted signal events increases with m_{vis} for large $|a_\tau|$ values, as shown in the ratio panels of figures 9 and 10 for an illustrative value of $a_\tau = 0.008$.

The combination of all final states and years, using SRs with $N_{\text{tracks}} = 0$ or 1, gives an observed best fit value of $a_\tau = 0.0009^{+0.0016}_{-0.0015}(\text{syst})^{+0.0028}_{-0.0027}(\text{stat})$, equivalent to $a_\tau = 0.0009^{+0.0032}_{-0.0031}$, at 68% confidence level (CL). The corresponding expected best fit value is $a_\tau = 0.0012^{+0.0041}_{-0.0043}$, as shown in figure 12(upper). Contrary to the signal strength measurement assuming SM values for a_τ and d_τ, the statistical uncertainty dominates in the measurement of a_τ because the sensitivity is driven by the high-m_{vis} bins where BSM effects could be enhanced. The corresponding observed (expected) constraint at 95% CL is: $-0.0042 < a_\tau < 0.0062$ ($-0.0051 < a_\tau < 0.0072$). The 68% CL constraint on d_τ is $|d_\tau| < 1.7 \times 10^{-17}\, e\,\text{cm}$ ($|d_\tau| < 2.3 \times 10^{-17}\, e\,\text{cm}$), with a best fit value of $d_\tau = 0.0 \times 10^{-17}\, e\,\text{cm}$, whereas the 95% CL interval is $|d_\tau| < 2.9 \times 10^{-17}\, e\,\text{cm}$ ($|d_\tau| < 3.4 \times 10^{-17}\, e\,\text{cm}$). These results are derived using events with $q^2 \to 0$, which is the kinematic value at which the electromagnetic dipole moments are defined. They are compared with constraints from other experiments in figure 13. If the measurement were performed using information about the m_{vis} distribution and with a floating normalization for the $\gamma\gamma \to \tau\tau$ process, the expected precision in the measurement of a_τ would decrease by about 50%.

The constraints on a_τ and d_τ can be converted to two-dimensional constraints on the real and imaginary parts of the Wilson coefficients $C_{\tau B}$ and $C_{\tau W}$ divided by Λ^2, using equation (5). The 95% CL intervals in the plane of the normalized Wilson coefficients are shown in figure 14.

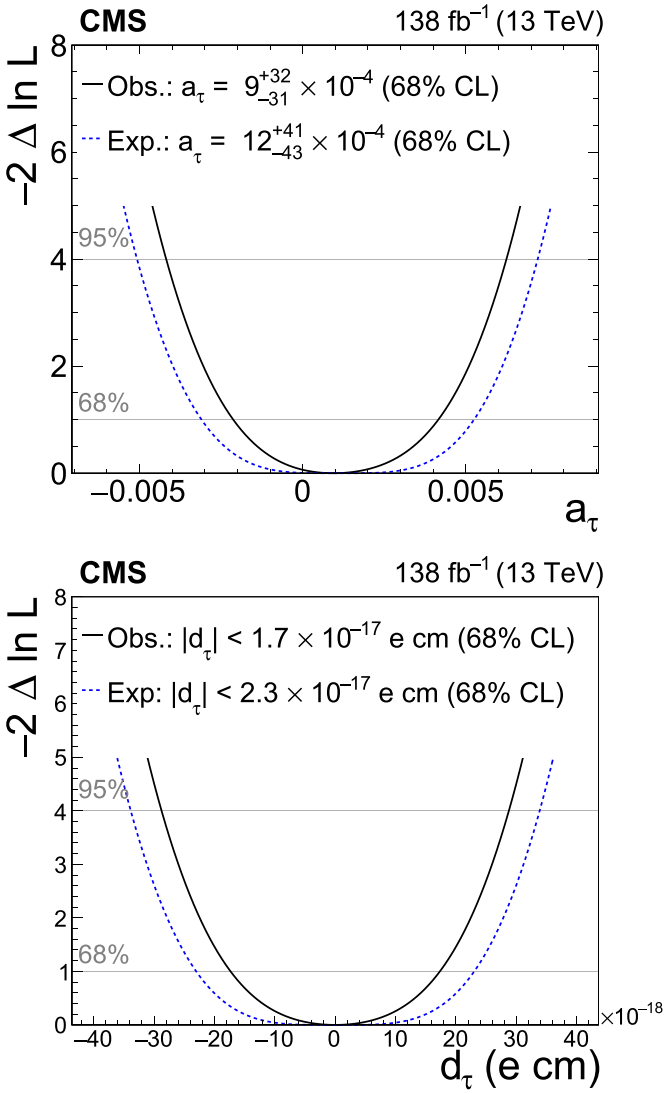

Figure 12. Expected and observed negative log-likelihood as a function of a_τ (upper) and d_τ (lower), for the combination of all SRs in all data-taking periods.

11. Summary

The photon-fusion production of a pair of τ leptons, $\gamma\gamma \to \tau\tau$, has been observed for the first time in proton–proton collisions, with a significance of 5.3 standard deviations. The τ leptons are reconstructed in their leptonic and hadronic decay modes. The signal has been identified by requiring low track activity around the di-τ vertex and low azimuthal acoplanarity between the τ candidates. Data in a CR with two muons were used to determine corrections for the simulations to accurately model the track multiplicity and to predict the signal contribution in the final state of two τ leptons. The signal strength, fiducial cross section, and constraints on the anomalous electromagnetic moments of the τ lepton have been extracted using the di-τ invariant mass distributions in four di-τ final states.

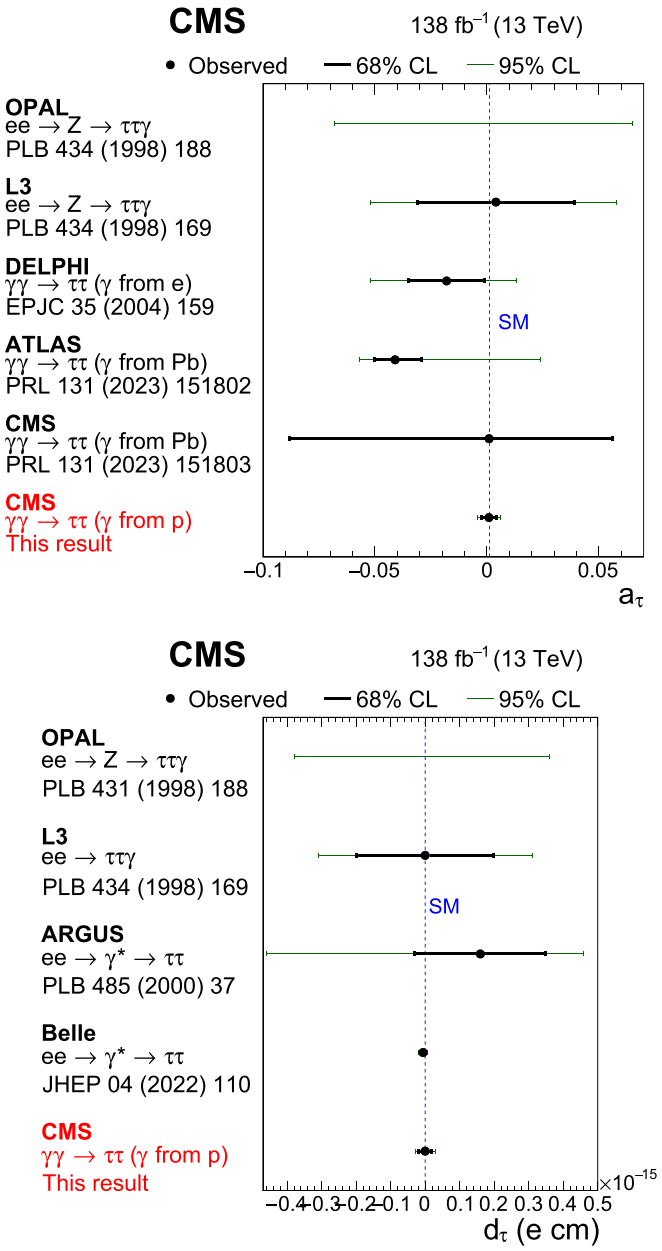

Figure 13. Measurements of a_τ (upper) and d_τ (lower) performed in this analysis, compared with previous results from the OPAL, L3, DELPHI, ARGUS, Belle, ATLAS, and CMS experiments [9, 10, 24–28]. Confidence intervals at 68 and 95% CL are shown with thick black and thin green lines, respectively. The SM values of the τ anomalous electromagnetic moments, $a_\tau = 1.2 \times 10^{-3}$ and $d_\tau = -7.3 \times 10^{-38}\, e\,\text{cm}$, are indicated with the dashed blue lines.

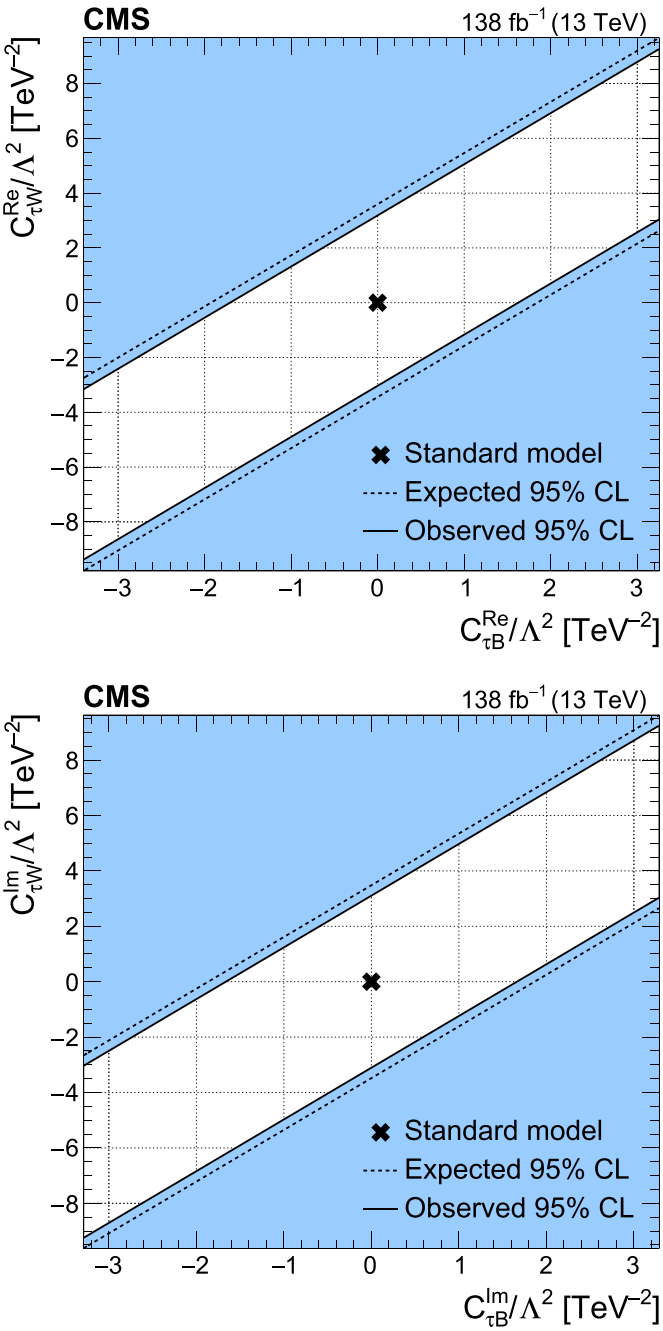

Figure 14. Expected and observed 95% CL constraints on the real (upper) and imaginary (lower) parts of the Wilson coefficients $C_{\tau B}$ and $C_{\tau W}$ divided by Λ^2. The SM value is indicated with a cross. The blue shaded areas indicate excluded regions.

The measured fiducial cross section of $\gamma\gamma \to \tau\tau$ is $\sigma_{\text{obs}}^{\text{fid}} = 12.4^{+3.8}_{-3.1}$ fb. The anomalous τ magnetic moment is determined to be $a_\tau = 0.0009^{+0.0032}_{-0.0031}$, whereas the electric dipole moment of the τ lepton is constrained to $|d_\tau| < 2.9 \times 10^{-17}\, e\,\text{cm}$ at 95% confidence level. They are both in good agreement with the predictions of the standard model of particle physics, and the measurements do not show any evidence for the presence of new physics that would modify the electromagnetic moments of the τ lepton. This is the most stringent limit on the τ lepton magnetic moment to date, improving on the previous best constraints by nearly an order of magnitude.

Data availability statement

Release and preservation of data used by the CMS Collaboration as the basis for publications is guided by the CMS data preservation, re-use and open access policy.

Acknowledgments

We congratulate our colleagues in the CERN accelerator departments for the excellent performance of the LHC and thank the technical and administrative staffs at CERN and at other CMS institutes for their contributions to the success of the CMS effort. In addition, we gratefully acknowledge the computing centers and personnel of the Worldwide LHC Computing Grid and other centers for delivering so effectively the computing infrastructure essential to our analyses. Finally, we acknowledge the enduring support for the construction and operation of the LHC, the CMS detector, and the supporting computing infrastructure provided by the following funding agencies: SC (Armenia), BMBWF and FWF (Austria); FNRS and FWO (Belgium); CNPq, CAPES, FAPERJ, FAPERGS, and FAPESP (Brazil); MES and BNSF (Bulgaria); CERN; CAS, MoST, and NSFC (China); MINCIENCIAS (Colombia); MSES and CSF (Croatia); RIF (Cyprus); SENESCYT (Ecuador); ERC PRG, RVTT3 and MoER TK202 (Estonia); Academy of Finland, MEC, and HIP (Finland); CEA and CNRS/IN2P3 (France); SRNSF (Georgia); BMBF, DFG, and HGF (Germany); GSRI (Greece); NKFIH (Hungary); DAE and DST (India); IPM (Iran); SFI (Ireland); INFN (Italy); MSIP and NRF (Republic of Korea); MES (Latvia); LMTLT (Lithuania); MOE and UM (Malaysia); BUAP, CINVESTAV, CONACYT, LNS, SEP, and UASLP-FAI (Mexico); MOS (Montenegro); MBIE (New Zealand); PAEC (Pakistan); MES and NSC (Poland); FCT (Portugal); MESTD (Serbia); MCIN/AEI and PCTI (Spain); MOSTR (Sri Lanka); Swiss Funding Agencies (Switzerland); MST (Taipei); MHESI and NSTDA (Thailand); TUBITAK and TENMAK (Turkey); NASU (Ukraine); STFC (United Kingdom); DOE and NSF (USA). Individuals have received support from the Marie-Curie program and the European Research Council and Horizon 2020 Grant, Contract Nos. 675440, 724704, 752730, 758316, 765710, 824093, 101115353, 101002207, and COST Action CA16108 (European Union); the Leventis Foundation; the Alfred P. Sloan Foundation; the Alexander von Humboldt Foundation; the Science Committee, Project No. 22rl-037 (Armenia); the Belgian Federal Science Policy Office; the Fonds pour la Formation à la Recherche dans l'Industrie et dans l'Agriculture (FRIA-Belgium); the Agentschap voor Innovatie door Wetenschap en Technologie (IWT-Belgium); the F.R.S.-FNRS and FWO (Belgium) under the 'Excellence of Science—EOS' – be.h project n. 30820817; the Beijing Municipal Science & Technology Commission, No. Z191100007219010 and Fundamental Research Funds for the Central Universities (China); the Ministry of Education, Youth and Sports (MEYS) of the Czech Republic; the Shota Rustaveli National Science Foundation, Grant FR-22-985 (Georgia); the Deutsche Forschungsgemeinschaft (DFG), under Germany's Excellence Strategy—EXC 2121 'Quantum Universe' – 390833306, and under Project Number 400140256–GRK2497; the Hellenic Foundation for Research and Innovation (HFRI), Project Number 2288 (Greece); the Hungarian Academy of Sciences, the New National Excellence Program–ÚNKP, the NKFIH research Grants K 131991, K 133046, K 138136, K 143460, K 143477, K 146913, K 146914, K 147048, 2020-2.2.1-ED-2021-00181, and TKP2021-NKTA-64 (Hungary); the Council of Science and Industrial Research, India; ICSC—National Research Center for High Performance Computing, Big Data and Quantum Computing and FAIR—Future Artificial Intelligence Research, funded by the NextGenerationEU program (Italy); the Latvian Council of Science; the Ministry of Education and Science, Project No. 2022/WK/14, and the National Science Center, Contracts Opus 2021/41/B/ST2/01369 and 2021/43/B/ST2/01552 (Poland); the Fundação para a Ciência e a Tecnologia, Grant CEECIND/01334/2018 (Portugal); the National Priorities Research Program by Qatar National Research Fund; MCIN/AEI/10.13039/501100011033, ERDF 'a way of making Europe', and the Programa Estatal de Fomento de la Investigación Científica y Técnica de Excelencia María de Maeztu, Grant MDM-2017-0765 and Programa Severo Ochoa del Principado de Asturias (Spain); the Chulalongkorn Academic into Its 2nd Century Project Advancement Project, and the National Science, Research and Innovation Fund via the Program Management Unit for Human Resources & Institutional Development, Research and Innovation, Grant B37G660013 (Thailand); the Kavli Foundation; the Nvidia Corporation; the SuperMicro Corporation; the Welch Foundation, contract C-1845; and the Weston Havens Foundation (USA).

The CMS Collaboration

A Hayrapetyan, A Tumasyan[1]
Yerevan Physics Institute, Yerevan, Armenia

W Adam, J W Andrejkovic, T Bergauer, S Chatterjee, K Damanakis, M Dragicevic, P S Hussain, M Jeitler[2], N Krammer, A Li, D Liko, I Mikulec, J Schieck[2], R Schöfbeck, D Schwarz, M Sonawane, S Templ, W Waltenberger, C -E Wulz[2]
Institut für Hochenergiephysik, Vienna, Austria

M R Darwish[3], T Janssen, P Van Mechelen
Universiteit Antwerpen, Antwerpen, Belgium

E S Bols, J D'Hondt, S Dansana, A De Moor, M Delcourt, H El Faham, S Lowette, I Makarenko, D Müller, A.R Sahasransu, S Tavernier, M Tytgat[4], G.P Van Onsem, S Van Putte, D Vannerom
Vrije Universiteit Brussel, Brussel, Belgium

B Clerbaux, A K Das, G De Lentdecker, L Favart, P Gianneios, D Hohov, J Jaramillo, A Khalilzadeh, K Lee, M Mahdavikhorrami, A Malara, S Paredes, N Postiau, L Thomas, M Vanden Bemden, C Vander Velde, P Vanlaer
Université Libre de Bruxelles, Bruxelles, Belgium

M De Coen, D Dobur, Y Hong, J Knolle, L Lambrecht, G Mestdach, K Mota Amarilo, C Rendón, A Samalan, K Skovpen, N Van Den Bossche, J van der Linden, L Wezenbeek
Ghent University, Ghent, Belgium

A Benecke, A Bethani, G Bruno, C Caputo, C Delaere, I S Donertas, A Giammanco, K Jaffel, Sa Jain, V Lemaitre, J Lidrych, P Mastrapasqua, K Mondal, T T Tran, S Wertz
Université Catholique de Louvain, Louvain-la-Neuve, Belgium

G A Alves, E Coelho, C Hensel, T Menezes De Oliveira, A Moraes, P Rebello Teles, M Soeiro
Centro Brasileiro de Pesquisas Fisicas, Rio de Janeiro, Brazil

W L Aldá Júnior, M Alves Gallo Pereira, M Barroso Ferreira Filho, H Brandao Malbouisson, W Carvalho, J Chinellato[5], E M Da Costa, G G Da Silveira[6], D De Jesus Damiao, S Fonseca De Souza, R Gomes De Souza, J Martins[7], C Mora Herrera, L Mundim, H Nogima, J P Pinheiro, A Santoro, A Sznajder, M Thiel, A Vilela Pereira
Universidade do Estado do Rio de Janeiro, Rio de Janeiro, Brazil

C A Bernardes[6], L Calligaris, T R Fernandez Perez Tomei, E M Gregores, P G Mercadante, S F Novaes, B Orzari, Sandra S Padula
Universidade Estadual Paulista, Universidade Federal do ABC, São Paulo, Brazil

A Aleksandrov, G Antchev, R Hadjiiska, P Iaydjiev, M Misheva, M Shopova, G Sultanov
Institute for Nuclear Research and Nuclear Energy, Bulgarian Academy of Sciences, Sofia, Bulgaria

A Dimitrov, L Litov, B Pavlov, P Petkov, A Petrov, E Shumka
University of Sofia, Sofia, Bulgaria

S Keshri, S Thakur
Instituto De Alta Investigación, Universidad de Tarapacá, Casilla 7 D, Arica, Chile

T Cheng, T Javaid, L Yuan
Beihang University, Beijing, People's Republic of China

Z Hu, J Liu, K Yi[8,9]
Department of Physics, Tsinghua University, Beijing, People's Republic of China

G.M Chen[10], H S Chen[10], M Chen[10], F Iemmi, C H Jiang, A Kapoor[11], H Liao, Z -A Liu[12], R Sharma[13], J N Song[12], J Tao, C Wang[10], J Wang, Z Wang[10], H Zhang
Institute of High Energy Physics, Beijing, People's Republic of China

A Agapitos, Y Ban, A Levin, C Li, Q Li, Y Mao, S J Qian, X Qin, X Sun, D Wang, H Yang, L Zhang, C Zhou
State Key Laboratory of Nuclear Physics and Technology, Peking University, Beijing, People's Republic of China

Z You
Sun Yat-Sen University, Guangzhou, People's Republic of China

N Lu
University of Science and Technology of People's Republic of China , Hefei, People's Republic of China

G Bauer[14]
Nanjing Normal University, Nanjing, People's Republic of China

X Gao[15], D Leggat, H Okawa
Institute of Modern Physics and Key Laboratory of Nuclear Physics and Ion-beam Application (MOE) - Fudan University, Shanghai, People's Republic of China

Z Lin, C Lu, M Xiao
Zhejiang University, Hangzhou, Zhejiang, People's Republic of China

C Avila, D A Barbosa Trujillo, A Cabrera, C Florez, J Fraga, J A Reyes Vega
Universidad de Los Andes, Bogota, Colombia

J Mejia Guisao, F Ramirez, M Rodriguez, J D Ruiz Alvarez
Universidad de Antioquia, Medellin, Colombia

D Giljanovic, N Godinovic, D Lelas, A Sculac
University of Split, Faculty of Electrical Engineering, Mechanical Engineering and Naval Architecture, Split, Croatia

M Kovac, T Sculac
University of Split, Faculty of Science, Split, Croatia

P Bargassa, V Brigljevic, B K Chitroda, D Ferencek, S Mishra, A Starodumov[16], T Susa
Institute Rudjer Boskovic, Zagreb, Croatia

A Attikis, K Christoforou, S Konstantinou, J Mousa, C Nicolaou, F Ptochos, P A Razis, H Rykaczewski, H Saka, A Stepennov
University of Cyprus, Nicosia, Cyprus

M Finger, M Finger Jr, A Kveton
Charles University, Prague, Czech Republic

E Ayala
Escuela Politecnica Nacional, Quito, Ecuador

E Carrera Jarrin
Universidad San Francisco de Quito, Quito, Ecuador

A A Abdelalim[17,18], E Salama[19,20]
Academy of Scientific Research and Technology of the Arab Republic of Egypt, Egyptian Network of High Energy Physics, Cairo, Egypt

A Lotfy, M A Mahmoud
Center for High Energy Physics (CHEP-FU), Fayoum University, El-Fayoum, Egypt

K Ehataht, M Kadastik, T Lange, S Nandan, C Nielsen, J Pata, M Raidal, L Tani, C Veelken
National Institute of Chemical Physics and Biophysics, Tallinn, Estonia

H Kirschenmann, K Osterberg, M Voutilainen
Department of Physics, University of Helsinki, Helsinki, Finland

S Bharthuar, E Brücken, F Garcia, K T S Kallonen, R Kinnunen, T Lampén, K Lassila-Perini, S Lehti, T Lindén, L Martikainen, M Myllymäki, M m Rantanen, H Siikonen, E Tuominen, J Tuominiemi
Helsinki Institute of Physics, Helsinki, Finland

P Luukka, H Petrow
Lappeenranta-Lahti University of Technology, Lappeenranta, Finland

M Besancon, F Couderc, M Dejardin, D Denegri, J L Faure, F Ferri, S Ganjour, P Gras, G Hamel de Monchenault, V Lohezic, J Malcles, J Rander, A Rosowsky, M.Ö Sahin, A Savoy-Navarro[21], P Simkina, M Titov, M Tornago
IRFU, CEA, Université Paris-Saclay, Gif-sur-Yvette, France

C Baldenegro Barrera, F Beaudette, A Buchot Perraguin, P Busson, A Cappati, C Charlot, M Chiusi, F Damas, O Davignon, A De Wit, B A Fontana Santos Alves, S Ghosh, A Gilbert, R Granier de Cassagnac, A Hakimi, B Harikrishnan, L Kalipoliti, G Liu, J Motta, M Nguyen, C Ochando, L Portales, R Salerno, J B Sauvan, Y Sirois, A Tarabini, E Vernazza, A Zabi, A Zghiche
Laboratoire Leprince-Ringuet, CNRS/IN2P3, Ecole Polytechnique, Institut Polytechnique de Paris, Palaiseau, France

J -L Agram[22], J Andrea, D Apparu, D Bloch, J -M Brom, E.C Chabert, C Collard, S Falke, U Goerlach, C Grimault, R Haeberle, A -C Le Bihan, M Meena, G Saha, M A Sessini, P Van Hove
Université de Strasbourg, CNRS, IPHC UMR 7178, Strasbourg, France

S Beauceron, B Blancon, G Boudoul, N Chanon, J Choi, D Contardo, P Depasse, C Dozen[23], H El Mamouni, J Fay, S Gascon, M Gouzevitch, C Greenberg, G Grenier, B Ille, I B Laktineh, M Lethuillier, L Mirabito, S Perries, A Purohit, M Vander Donckt, P Verdier, J Xiao
Institut de Physique des 2 Infinis de Lyon (IP2I), Villeurbanne, France

D Chokheli, I Lomidze, Z Tsamalaidze[16]
Georgian Technical University, Tbilisi, Georgia

V Botta, L Feld, K Klein, M Lipinski, D Meuser, A Pauls, N Röwert, M Teroerde
RWTH Aachen University, I. Physikalisches Institut, Aachen, Germany

S Diekmann, A Dodonova, N Eich, D Eliseev, F Engelke, J Erdmann, M Erdmann, P Fackeldey, B Fischer, T Hebbeker, K Hoepfner, F Ivone, A Jung, M y Lee, L Mastrolorenzo, F Mausolf, M Merschmeyer, A Meyer, S Mukherjee, D Noll, F Nowotny, A Pozdnyakov, Y Rath, W Redjeb, F Rehm, H Reithler, U Sarkar, V Sarkisovi, A Schmidt, A Sharma, J L Spah, A Stein, F Torres Da Silva De Araujo[24], L Vigilante, S Wiedenbeck, S Zaleski
RWTH Aachen University, III. Physikalisches Institut A, Aachen, Germany

C Dziwok, G Flügge, W Haj Ahmad[25], T Kress, A Nowack, O Pooth, A Stahl, T Ziemons, A Zotz
RWTH Aachen University, III. Physikalisches Institut B, Aachen, Germany

H Aarup Petersen, M Aldaya Martin, J Alimena, S Amoroso, Y An, S Baxter, M Bayatmakou, H Becerril Gonzalez, O Behnke, A Belvedere, S Bhattacharya, F Blekman[26], K Borras[27], A Campbell, A Cardini, C Cheng, F Colombina, S Consuegra Rodríguez, G Correia Silva, M De Silva, G Eckerlin, D Eckstein, L I Estevez Banos, O Filatov, E Gallo[26], A Geiser, A Giraldi, G Greau, V Guglielmi, M Guthoff, A Hinzmann, A Jafari[28], L Jeppe, N Z Jomhari, B Kaech, M Kasemann, C Kleinwort, R Kogler, M Komm, D Krücker, W Lange, D Leyva Pernia, K Lipka[29], W Lohmann[30], R Mankel, I -A Melzer-Pellmann, M Mendizabal Morentin, A B Meyer, G Milella, A Mussgiller, L P Nair, A Nürnberg, Y Otarid, J Park, D Pérez Adán, E Ranken, A Raspereza, B Ribeiro Lopes, J Rübenach, A Saggio, M Scham[31,27], S Schnake[27], P Schütze, C Schwanenberger[26], D Selivanova, K Sharko, M Shchedrolosiev, R E Sosa Ricardo, D Stafford, F Vazzoler, A Ventura Barroso, R Walsh, Q Wang, Y Wen, K Wichmann, L Wiens[27], C Wissing, Y Yang, A Zimermmane Castro Santos
Deutsches Elektronen-Synchrotron, Hamburg, Germany

A Albrecht, S Albrecht, M Antonello, S Bein, L Benato, S Bollweg, M Bonanomi, P Connor, M Eich, K El Morabit, Y Fischer, A Fröhlich, C Garbers, E Garutti, A Grohsjean, M Hajheidari, J Haller, H R Jabusch, G Kasieczka, P Keicher, R Klanner, W Korcari, T Kramer, V Kutzner, F Labe, J Lange, A Lobanov, C Matthies, A Mehta, L Moureaux, M Mrowietz, A Nigamova, Y Nissan, A Paasch, K J Pena Rodriguez, T Quadfasel, B Raciti, M Rieger, D Savoiu, J Schindler, P Schleper, M Schröder, J Schwandt, M Sommerhalder, H Stadie, G Steinbrück, A Tews, M Wolf
University of Hamburg, Hamburg, Germany

S Brommer, M Burkart, E Butz, T Chwalek, A Dierlamm, A Droll, N Faltermann, M Giffels, A Gottmann, F Hartmann[32], R Hofsaess, M Horzela, U Husemann, J Kieseler, M Klute, R Koppenhöfer, J M Lawhorn, M Link, A Lintuluoto, S Maier, S Mitra, M Mormile, Th Müller, M Neukum, M Oh, M Presilla, G Quast, K Rabbertz, B Regnery, N Shadskiy, I Shvetsov, H J Simonis, M Toms, N Trevisani, R Ulrich, R F Von Cube, M Wassmer, S Wieland, F Wittig, R Wolf, X Zuo
Karlsruher Institut fuer Technologie, Karlsruhe, Germany

G Anagnostou, G Daskalakis, A Kyriakis, A Papadopoulos[32], A Stakia
Institute of Nuclear and Particle Physics (INPP), NCSR Demokritos, Aghia Paraskevi, Greece

P Kontaxakis, G Melachroinos, A Panagiotou, I Papavergou, I Paraskevas, N Saoulidou, K Theofilatos, E Tziaferi, K Vellidis, I Zisopoulos
National and Kapodistrian University of Athens, Athens, Greece

G Bakas, T Chatzistavrou, G Karapostoli, K Kousouris, I Papakrivopoulos, E Siamarkou, G Tsipolitis, A Zacharopoulou
National Technical University of Athens, Athens, Greece

K Adamidis, I Bestintzanos, I Evangelou, C Foudas, C Kamtsikis, P Katsoulis, P Kokkas, P G Kosmoglou Kioseoglou, N Manthos, I Papadopoulos, J Strologas
University of Ioánnina, Ioánnina, Greece

M Bartók[33], C Hajdu, D Horvath[34,35], K Márton, F Sikler, V Veszpremi
HUN-REN Wigner Research Centre for Physics, Budapest, Hungary

M Csanád, K Farkas, M M A Gadallah[36], Á Kadlecsik, P Major, K Mandal, G Pásztor, A.J Rádl[37], G.I Veres
MTA-ELTE Lendület CMS Particle and Nuclear Physics Group, Eötvös Loránd University, Budapest, Hungary

P Raics, B Ujvari, G Zilizi
Faculty of Informatics, University of Debrecen, Debrecen, Hungary

G Bencze, S Czellar, J Molnar, Z Szillasi
Institute of Nuclear Research ATOMKI, Debrecen, Hungary

T Csorgo[37], F Nemes[37], T Novak
Karoly Robert Campus, MATE Institute of Technology, Gyongyos, Hungary

J Babbar, S Bansal, S.B Beri, V Bhatnagar, G Chaudhary, S Chauhan, N Dhingra[38], A Kaur, A Kaur, H Kaur, M Kaur, S Kumar, K Sandeep, T Sheokand, J B Singh, A Singla
Panjab University, Chandigarh, India

A Ahmed, A Bhardwaj, A Chhetri, B C Choudhary, A Kumar, A Kumar, M Naimuddin, K Ranjan, S Saumya
University of Delhi, Delhi, India

S Baradia, S Barman[39], S Bhattacharya, S Dutta, S Dutta, S Sarkar
Saha Institute of Nuclear Physics, HBNI, Kolkata, India

M M Ameen, P K Behera, S C Behera, S Chatterjee, P Jana, P Kalbhor, J R Komaragiri[40], D Kumar[40], L Panwar[40], P R Pujahari, N R Saha, A Sharma, A K Sikdar, S Verma
Indian Institute of Technology Madras, Madras, India

S Dugad, M Kumar, G B Mohanty, P Suryadevara
Tata Institute of Fundamental Research-A, Mumbai, India

A Bala, S Banerjee, R M Chatterjee, R K Dewanjee[41], M Guchait, Sh Jain, A Jaiswal, S Karmakar, S Kumar, G Majumder, K Mazumdar, S Parolia, A Thachayath
Tata Institute of Fundamental Research-B, Mumbai, India

S Bahinipati[42], C Kar, D Maity[43], P Mal, T Mishra, V K Muraleedharan Nair Bindhu[43], K Naskar[43], A Nayak[43], P Sadangi, P Saha, S K Swain, S Varghese[43], D Vats[43]
National Institute of Science Education and Research, An OCC of Homi Bhabha National Institute, Bhubaneswar, Odisha, India

S Acharya[44], A Alpana, S Dube, B Gomber[44], B Kansal, A Laha, B Sahu[44], S Sharma, K Y Vaish
Indian Institute of Science Education and Research (IISER), Pune, India

H Bakhshiansohi[45], E Khazaie[46], M Zeinali[47]
Isfahan University of Technology, Isfahan, Iran

S Chenarani[48], S M Etesami, M Khakzad, M Mohammadi Najafabadi
Institute for Research in Fundamental Sciences (IPM), Tehran, Iran

M Grunewald
University College Dublin, Dublin, Ireland

M Abbrescia[a,b], R Aly[a,c,17], A Colaleo[a,b], D Creanza[a,c], B D'Anzi[a,b], N De Filippis[a,c], M De Palma[a,b], A Di Florio[a,c], W Elmetenawee[a,b,17], L Fiore[a], G Iaselli[a,c], M Louka[a,b], G Maggi[a,c], M Maggi[a], I Margjeka[a,b], V Mastrapasqua[a,b], S My[a,b], S Nuzzo[a,b], A Pellecchia[a,b], A Pompili[a,b], G Pugliese[a,c], R Radogna[a], G Ramirez-Sanchez[a,c], D Ramos[a], A Ranieri[a], L Silvestris[a], F M Simone[a,b], Ü Sözbilir[a], A Stamerra[a], R Venditti[a], P Verwilligen[a], A Zaza[a,b]
INFN Sezione di Bari[a], Università di Bari[b], Politecnico di Bari[c], Bari, Italy

G Abbiendi[a], C Battilana[a,b], D Bonacorsi[a,b], L Borgonovi[a], R Campanini[a,b], P Capiluppi[a,b], A Castro[a,b], F R Cavallo[a], M Cuffiani[a,b], T Diotalevi[a,b], F Fabbri[a], A Fanfani[a,b], D Fasanella[a,b], P Giacomelli[a], L Giommi[a,b], C Grandi[a], L Guiducci[a,b], S Lo Meo[a,49], L Lunerti[a,b], S Marcellini[a], G Masetti[a], F L Navarria[a,b], A Perrotta[a], F Primavera[a,b], A M Rossi[a,b], T Rovelli[a,b], G P Siroli[a,b]
INFN Sezione di Bologna[a], Università di Bologna[b], Bologna, Italy

S Costa[a,b,50], A Di Mattia[a], R Potenza[a,b], A Tricomi[a,b,50], C Tuve[a,b]
INFN Sezione di Catania[a], Università di Catania[b], Catania, Italy

P Assiouras[a], G Barbagli[a], G Bardelli[a,b], B Camaiani[a,b], A Cassese[a], R Ceccarelli[a], V Ciulli[a,b], C Civinini[a], R D'Alessandro[a,b], E Focardi[a,b], T Kello[a], G Latino[a,b], P Lenzi[a,b], M Lizzo[a], M Meschini[a], S Paoletti[a], A Papanastassiou[a,b], G Sguazzoni[a], L Viliani[a]
INFN Sezione di Firenze[a], Università di Firenze[b], Firenze, Italy

L Benussi, S Bianco, S Meola[51], D Piccolo
INFN Laboratori Nazionali di Frascati, Frascati, Italy

P Chatagnon[a], F Ferro[a], E Robutti[a], S Tosi[a,b]
INFN Sezione di Genova[a], Università di Genova[b], Genova, Italy

A Benaglia[a], G Boldrini[a,b], F Brivio[a], F Cetorelli[a], F De Guio[a,b], M E Dinardo[a,b], P Dini[a], S Gennai[a], R Gerosa[a,b], A Ghezzi[a,b], P Govoni[a,b], L Guzzi[a], M T Lucchini[a,b], M Malberti[a], S Malvezzi[a], A Massironi[a], D Menasce[a], L Moroni[a], M Paganoni[a,b], D Pedrini[a], B S Pinolini[a], S Ragazzi[a,b], T Tabarelli de Fatis[a,b], D Zuolo[a]
INFN Sezione di Milano-Bicocca[a], Università di Milano-Bicocca[b], Milano, Italy

S Buontempo[a], A Cagnotta[a,b], F Carnevali[a,b], N Cavallo[a,c], F Fabozzi[a,c], A O M Iorio[a,b], L Lista[a,b,52], P Paolucci[a,32], B Rossi[a], C Sciacca[a,b]
INFN Sezione di Napoli[a], Università di Napoli 'Federico II'[b], Napoli, Italy; Università della Basilicata[c], Potenza, Italy; Scuola Superiore Meridionale (SSM)[d], Napoli, Italy

R Ardino[a], P Azzi[a], N Bacchetta[a,53], P Bortignon[a], A Bragagnolo[a,b], R Carlin[a,b], P Checchia[a], T Dorigo[a], F Gasparini[a,b], U Gasparini[a,b], E Lusiani[a], M Margoni[a,b], F Marini[a], A T Meneguzzo[a,b], M Migliorini[a,b], F Montecassiano[a], J Pazzini[a,b], P Ronchese[a,b], R Rossin[a,b], F Simonetto[a,b], G Strong[a], M Tosi[a,b], A Triossi[a,b], S Ventura[a], H Yarar[a,b], M Zanetti[a,b], P Zotto[a,b], A Zucchetta[a,b], G Zumerle[a,b]
INFN Sezione di Padova[a], Università di Padova[b], Padova, Italy; Università di Trento[c], Trento, Italy

S Abu Zeid[a,20], C Aimè[a,b], A Braghieri[a], S Calzaferri[a], D Fiorina[a], P Montagna[a,b], V Re[a], C Riccardi[a,b], P Salvini[a], I Vai[a,b], P Vitulo[a,b]
INFN Sezione di Pavia[a], Università di Pavia[b], Pavia, Italy

S Ajmal[a,b], G M Bilei[a], D Ciangottini[a,b], L Fanò[a,b], M Magherini[a,b], G Mantovani[a,b], V Mariani[a,b], M Menichelli[a], F Moscatelli[a,54], A Rossi[a,b], A Santocchia[a,b], D Spiga[a], T Tedeschi[a,b]
INFN Sezione di Perugia[a], Università di Perugia[b], Perugia, Italy

P Asenov[a,b], P Azzurri[a], G Bagliesi[a], R Bhattacharya[a], L Bianchini[a,b], T Boccali[a], E Bossini[a], D Bruschini[a,c], R Castaldi[a], M A Ciocci[a,b], M Cipriani[a,b], V D'Amante[a,d], R Dell'Orso[a], S Donato[a], A Giassi[a], F Ligabue[a,c], D Matos Figueiredo[a], A Messineo[a,b], M Musich[a,b], F Palla[a], A Rizzi[a,b], G Rolandi[a,c], S Roy Chowdhury[a], T Sarkar[a], A Scribano[a], P Spagnolo[a], R Tenchini[a], G Tonelli[a,b], N Turini[a,d], A Venturi[a], P G Verdini[a]
INFN Sezione di Pisa[a], Università di Pisa[b], Scuola Normale Superiore di Pisa[c], Pisa, Italy; Università di Siena[d], Siena, Italy

P Barria[a], M Campana[a,b], F Cavallari[a], L Cunqueiro Mendez[a,b], D Del Re[a,b], E Di Marco[a], M Diemoz[a], F Errico[a,b], E Longo[a,b], P Meridiani[a], J Mijuskovic[a,b], G Organtini[a,b], F Pandolfi[a], R Paramatti[a,b], C Quaranta[a,b], S Rahatlou[a,b], C Rovelli[a], F Santanastasio[a,b], L Soffi[a]
INFN Sezione di Roma[a], Sapienza Università di Roma[b], Roma, Italy

N Amapane[a,b], R Arcidiacono[a,c], S Argiro[a,b], M Arneodo[a,c], N Bartosik[a], R Bellan[a,b], A Bellora[a,b], C Biino[a], C Borca[a,b], N Cartiglia[a], M Costa[a,b], R Covarelli[a,b], N Demaria[a], L Finco[a], M Grippo[a,b], B Kiani[a,b], F Legger[a], F Luongo[a,b], C Mariotti[a], L Markovic[a,b], S Maselli[a], A Mecca[a,b], E Migliore[a,b], M Monteno[a], R Mulargia[a], M M Obertino[a,b], G Ortona[a], L Pacher[a,b], N Pastrone[a], M Pelliccioni[a], M Ruspa[a,c], F Siviero[a,b], V Sola[a,b], A Solano[a,b], A Staiano[a], C Tarricone[a,b], D Trocino[a], G Umoret[a,b], E Vlasov[a,b]
INFN Sezione di Torino[a], Università di Torino[b], Torino, Italy; Università del Piemonte Orientale[c], Novara, Italy

S Belforte[a], V Candelise[a,b], M Casarsa[a], F Cossutti[a], K De Leo[a,b], G Della Ricca[a,b]
INFN Sezione di Trieste[a], Università di Trieste[b], Trieste, Italy

S Dogra, J Hong, C Huh, B Kim, D.H Kim, J Kim, H Lee, S.W Lee, C.S Moon, Y.D Oh, M.S Ryu, S Sekmen, Y.C Yang
Kyungpook National University, Daegu, Republic of Korea

M S Kim
Department of Mathematics and Physics - GWNU, Gangneung, Republic of Korea

G Bak, P Gwak, H Kim, D H Moon
Chonnam National University, Institute for Universe and Elementary Particles, Kwangju, Republic of Korea

E Asilar, D Kim, T J Kim, J A Merlin
Hanyang University, Seoul, Republic of Korea

S Choi, S Han, B Hong, K Lee, K S Lee, S Lee, J Park, S K Park, J Yoo
Republic of Korea University, Seoul, Republic of Korea

J Goh, S Yang
Kyung Hee University, Department of Physics, Seoul, Republic of Korea

H S Kim, Y Kim, S Lee
Sejong University, Seoul, Republic of Korea

J Almond, J H Bhyun, J Choi, W Jun, J Kim, S Ko, H Kwon, H Lee, J Lee, J Lee, B H Oh, S B Oh, H Seo, U K Yang, I Yoon
Seoul National University, Seoul, Republic of Korea

W Jang, D Y Kang, Y Kang, S Kim, B Ko, J S H Lee, Y Lee, I C Park, Y Roh, I.J Watson
University of Seoul, Seoul, Republic of Korea

S Ha, H D Yoo
Yonsei University, Department of Physics, Seoul, Republic of Korea

M Choi, M R Kim, H Lee, Y Lee, I Yu
Sungkyunkwan University, Suwon, Republic of Korea

T Beyrouthy, Y Maghrbi
College of Engineering and Technology, American University of the Middle East (AUM), Dasman, Kuwait

K Dreimanis, A Gaile, G Pikurs, A Potrebko, M Seidel, V Veckalns[55]
Riga Technical University, Riga, Latvia

N R Strautnieks
University of Latvia (LU), Riga, Latvia

M Ambrozas, A Juodagalvis, A Rinkevicius, G Tamulaitis
Vilnius University, Vilnius, Lithuania

N Bin Norjoharuddeen, I Yusuff[56], Z Zolkapli
National Centre for Particle Physics, Universiti Malaya, Kuala Lumpur, Malaysia

J F Benitez, A Castaneda Hernandez, H A Encinas Acosta, L G Gallegos Maríñez, M León Coello, J A Murillo Quijada, A Sehrawat, L Valencia Palomo
Universidad de Sonora (UNISON), Hermosillo, Mexico

G Ayala, H Castilla-Valdez, H Crotte Ledesma, E De La Cruz-Burelo, I Heredia-De La Cruz[57], R Lopez-Fernandez, C A Mondragon Herrera, A Sánchez Hernández
Centro de Investigacion y de Estudios Avanzados del IPN, Mexico City, Mexico

C Oropeza Barrera, M Ramírez García
Universidad Iberoamericana, Mexico City, Mexico

I Bautista, I Pedraza, H A Salazar Ibarguen, C Uribe Estrada
Benemerita Universidad Autonoma de Puebla, Puebla, Mexico

I Bubanja, N Raicevic
University of Montenegro, Podgorica, Montenegro

P H Butler
University of Canterbury, Christchurch, New Zealand

A Ahmad, M I Asghar, A Awais, M I M Awan, H R Hoorani, W A Khan
National Centre for Physics, Quaid-I-Azam University, Islamabad, Pakistan

V Avati, L Grzanka, M Malawski
AGH University of Krakow, Faculty of Computer Science, Electronics and Telecommunications, Krakow, Poland

H Bialkowska, M Bluj, B Boimska, M Górski, M Kazana, M Szleper, P Zalewski
National Centre for Nuclear Research, Swierk, Poland

K Bunkowski, K Doroba, A Kalinowski, M Konecki, J Krolikowski, A Muhammad
Institute of Experimental Physics, Faculty of Physics, University of Warsaw, Warsaw, Poland

K Pozniak, W Zabolotny
Warsaw University of Technology, Warsaw, Poland

M Araujo, D Bastos, C Beirão Da Cruz E Silva, A Boletti, M Bozzo, T Camporesi, G Da Molin, P Faccioli, M Gallinaro, J Hollar, N Leonardo, T Niknejad, A Petrilli, M Pisano, J Seixas, J Varela, J W Wulff
Laboratório de Instrumentação e Física Experimental de Partículas, Lisboa, Portugal

P Adzic, P Milenovic
Faculty of Physics, University of Belgrade, Belgrade, Serbia

M Dordevic, J Milosevic, V Rekovic
VINCA Institute of Nuclear Sciences, University of Belgrade, Belgrade, Serbia

M Aguilar-Benitez, J Alcaraz Maestre, Cristina F Bedoya, M Cepeda, M Cerrada, N Colino, B De La Cruz, A Delgado Peris, A Escalante Del Valle, D Fernández Del Val, J P Fernández Ramos, J Flix, M C Fouz, O Gonzalez Lopez, S Goy Lopez, J M Hernandez, M I Josa, D Moran, C M Morcillo Perez, Á Navarro Tobar, C Perez Dengra, A Pérez-Calero Yzquierdo, J Puerta Pelayo, I Redondo, D D Redondo Ferrero, L Romero, S Sánchez Navas, L Urda Gómez, J Vazquez Escobar, C Willmott
Centro de Investigaciones Energéticas Medioambientales y Tecnológicas (CIEMAT), Madrid, Spain

J F de Trocóniz
Universidad Autónoma de Madrid, Madrid, Spain

B Alvarez Gonzalez, J Cuevas, J Fernandez Menendez, S Folgueras, I Gonzalez Caballero, J R González Fernández, E Palencia Cortezon, C Ramón Álvarez, V Rodríguez Bouza, A Soto Rodríguez, A Trapote, C Vico Villalba, P Vischia
Universidad de Oviedo, Instituto Universitario de Ciencias y Tecnologías Espaciales de Asturias (ICTEA), Oviedo, Spain

S Bhowmik, S Blanco Fernández, J A Brochero Cifuentes, I J Cabrillo, A Calderon, J Duarte Campderros, M Fernandez, G Gomez, C Lasaosa García, C Martinez Rivero, P Martinez Ruiz del Arbol, F Matorras, P Matorras Cuevas, E Navarrete Ramos, J Piedra Gomez, L Scodellaro, I Vila, J M Vizan Garcia
Instituto de Física de Cantabria (IFCA), CSIC-Universidad de Cantabria, Santander, Spain

M K Jayananda, B Kailasapathy[58], D U J Sonnadara, D D C Wickramarathna
University of Colombo, Colombo, Sri Lanka

W G D Dharmaratna[59], K Liyanage, N Perera, N Wickramage
University of Ruhuna, Department of Physics, Matara, Sri Lanka

D Abbaneo, C Amendola, E Auffray, G Auzinger, J Baechler, D Barney, A Bermúdez Martínez, M Bianco, B Bilin, A A Bin Anuar, A Bocci, C Botta, E Brondolin, C Caillol, G Cerminara, N Chernyavskaya, D d'Enterria, A Dabrowski, A David, A De Roeck, M M Defranchis, M Deile, M Dobson, L Forthomme, G Franzoni, W Funk, S Giani, D Gigi, K Gill, F Glege, L Gouskos, M Haranko, J Hegeman, B Huber, V Innocente, T James, P Janot, S Laurila, P Lecoq, E Leutgeb, C Lourenço, B Maier, L Malgeri, M Mannelli, A C Marini, M Matthewman, F Meijers, S Mersi, E Meschi, V Milosevic, F Monti, F Moortgat, M Mulders, I Neutelings, S Orfanelli, F Pantaleo, G Petrucciani, A Pfeiffer, M Pierini, D Piparo, H Qu, D Rabady, G Reales Gutiérrez, M Rovere, H Sakulin, S Scarfi, C Schwick, M Selvaggi, A Sharma, K Shchelina, P Silva, P Sphicas[60], A G Stahl Leiton, A Steen, S Summers, D Treille, P Tropea, A Tsirou, D Walter, J Wanczyk[61], J Wang, S Wuchterl, P Zehetner, P Zejdl, W D Zeuner
CERN, European Organization for Nuclear Research, Geneva, Switzerland

T Bevilacqua[62], L Caminada[62], A Ebrahimi, W Erdmann, R Horisberger, Q Ingram, H C Kaestli, D Kotlinski, C Lange, M Missiroli[62], L Noehte[62], T Rohe
Paul Scherrer Institut, Villigen, Switzerland

T K Aarrestad, K Androsov[61], M Backhaus, A Calandri, C Cazzaniga, K Datta, A De Cosa, G Dissertori, M Dittmar, M Donegà, F Eble, M Galli, K Gedia, F Glessgen, C Grab, D Hits, W Lustermann, A -M Lyon, R A Manzoni, M Marchegiani, L Marchese, C Martin Perez, A Mascellani[61], F Nessi-Tedaldi, F Pauss, V Perovic, S Pigazzini, C Reissel, T Reitenspiess, B Ristic, F Riti, D Ruini, R Seidita, J Steggemann[61], D Valsecchi, R Wallny
ETH Zurich - Institute for Particle Physics and Astrophysics (IPA), Zurich, Switzerland

C Amsler[63], P Bärtschi, D Brzhechko, M.F Canelli, K Cormier, J K Heikkilä, M Huwiler, W Jin, A Jofrehei, B Kilminster, S Leontsinis, S P Liechti, A Macchiolo, P Meiring, U Molinatti, A Reimers, P Robmann, S Sanchez Cruz, M Senger, Y Takahashi, R Tramontano
Universität Zürich, Zurich, Switzerland

C Adloff[64], D Bhowmik, C M Kuo, W Lin, P K Rout, P C Tiwari[40], S S Yu
National Central University, Chung-Li, Taiwan

L Ceard, Y Chao, K F Chen, P s Chen, Z g Chen, A De Iorio, W -S Hou, T h Hsu, Y w Kao, R Khurana, G Kole, Y y Li, R -S Lu, E Paganis, X f Su, J Thomas-Wilsker, L s Tsai, H y Wu, E Yazgan
National Taiwan University (NTU), Taipei, Taiwan

C Asawatangtrakuldee, N Srimanobhas, V Wachirapusitanand
High Energy Physics Research Unit, Department of Physics, Faculty of Science, Chulalongkorn University, Bangkok, Thailand

D Agyel, F Boran, Z S Demiroglu, F Dolek, I Dumanoglu[65], E Eskut, Y Guler[66], E Gurpinar Guler[66], C Isik, O Kara, A Kayis Topaksu, U Kiminsu, G Onengut, K Ozdemir[67], A Polatoz, B Tali[68], U G Tok, S Turkcapar, E Uslan, I S Zorbakir
Çukurova University, Physics Department, Science and Art Faculty, Adana, Turkey

M Yalvac[69]
Middle East Technical University, Physics Department, Ankara, Turkey

B Akgun, I O Atakisi, E Gülmez, M Kaya[70], O Kaya[71], S Tekten[72]
Bogazici University, Istanbul, Turkey

A Cakir, K Cankocak[65,73], Y Komurcu, S Sen[74]
Istanbul Technical University, Istanbul, Turkey

O Aydilek, S Cerci[68], V Epshteyn, B Hacisahinoglu, I Hos[75], B Kaynak, S Ozkorucuklu, O Potok, H Sert, C Simsek, C Zorbilmez
Istanbul University, Istanbul, Turkey

B Isildak[76], D Sunar Cerci[68]
Yildiz Technical University, Istanbul, Turkey

A Boyaryntsev, B Grynyov
Institute for Scintillation Materials of National Academy of Science of Ukraine, Kharkiv, Ukraine

L Levchuk
National Science Centre, Kharkiv Institute of Physics and Technology, Kharkiv, Ukraine

D Anthony, J J Brooke, A Bundock, F Bury, E Clement, D Cussans, H Flacher, M Glowacki, J Goldstein, H F Heath, L Kreczko, S Paramesvaran, L Robertshaw, S Seif El Nasr-Storey, V J Smith, N Stylianou[77], K Walkingshaw Pass, R White
University of Bristol, Bristol, United Kingdom

A H Ball, K W Bell, A Belyaev[78], C Brew, R M Brown, D J A Cockerill, C Cooke, K V Ellis, K Harder, S Harper, M -L Holmberg[79], J Linacre, K Manolopoulos, D M Newbold, E Olaiya, D Petyt, T Reis, G Salvi, T Schuh, C H Shepherd-Themistocleous, I R Tomalin, T Williams
Rutherford Appleton Laboratory, Didcot, United Kingdom

R Bainbridge, P Bloch, C E Brown, O Buchmuller, V Cacchio, C A Carrillo Montoya, G S Chahal[80], D Colling, J S Dancu, I Das, P Dauncey, G Davies, J Davies, M Della Negra, S Fayer, G Fedi, G Hall, M H Hassanshahi, A Howard, G Iles, M Knight, J Langford, J León Holgado, L Lyons, A -M Magnan, S Malik, M Mieskolainen, J Nash[81], M Pesaresi, B C Radburn-Smith, A Richards, A Rose, K Savva, C Seez, R Shukla, A Tapper, K Uchida, G P Uttley, L H Vage, T Virdee[32], M Vojinovic, N Wardle, D Winterbottom
Imperial College, London, United Kingdom

K Coldham, J E Cole, A Khan, P Kyberd, I D Reid
Brunel University, Uxbridge, United Kingdom

S Abdullin, A Brinkerhoff, B Caraway, J Dittmann, K Hatakeyama, J Hiltbrand, B McMaster, M Saunders, S Sawant, C Sutantawibul, J Wilson
Baylor University, Waco, Texas, United States of America

R Bartek, A Dominguez, C Huerta Escamilla, A E Simsek, R Uniyal, A M Vargas Hernandez
Catholic University of America, Washington, DC, United States of America

B Bam, R Chudasama, S I Cooper, S V Gleyzer, C U Perez, P Rumerio[82], E United States of Americai, R Yi
The University of Alabama, Tuscaloosa, Alabama, United States of America

A Akpinar, D Arcaro, C Cosby, Z Demiragli, C Erice, C Fangmeier, C Fernandez Madrazo, E Fontanesi, D Gastler, F Golf, S Jeon, I Reed, J Rohlf, K Salyer, D Sperka, D Spitzbart, I Suarez, A Tsatsos, S Yuan, A G Zecchinelli
Boston University, Boston, Massachusetts, United States of America

G Benelli, X Coubez[27], D Cutts, M Hadley, U Heintz, J M Hogan[83], T Kwon, G Landsberg, K T Lau, D Li, J Luo, S Mondal, M Narain[†], N Pervan, S Sagir[84], F Simpson, M Stamenkovic, W Y Wong, X Yan, W Zhang
Brown University, Providence, Rhode Island, United States of America

S Abbott, J Bonilla, C Brainerd, R Breedon, M Calderon De La Barca Sanchez, M Chertok, M Citron, J Conway, P.T Cox, R Erbacher, F Jensen, O Kukral, G Mocellin, M Mulhearn, D Pellett, W Wei, Y Yao, F Zhang
University of California, Davis, Davis, California, United States of America

M Bachtis, R Cousins, A Datta, G Flores Avila, J Hauser, M Ignatenko, M A Iqbal, T Lam, E Manca, A Nunez Del Prado, D Saltzberg, V Valuev
University of California, Los Angeles, California, United States of America

R Clare, J W Gary, M Gordon, G Hanson, W Si, S Wimpenny[†]
University of California, Riverside, Riverside, California, United States of America

J.G Branson, S Cittolin, S Cooperstein, D Diaz, J Duarte, L Giannini, J Guiang, R Kansal, V Krutelyov, R Lee, J Letts, M Masciovecchio, F Mokhtar, S Mukherjee, M Pieri, M Quinnan, B V Sathia Narayanan, V Sharma, M Tadel, E Vourliotis, F Würthwein, Y Xiang, A Yagil
University of California, San Diego, La Jolla, California, United States of America

A Barzdukas, L Brennan, C Campagnari, A Dorsett, J Incandela, J Kim, A J Li, P Masterson, H Mei, J Richman, U Sarica, R Schmitz, F Setti, J Sheplock, D Stuart, T Á Vámi, S Wang
University of California, Santa Barbara - Department of Physics, Santa Barbara, California, United States of America

A Bornheim, O Cerri, A Latorre, J Mao, H B Newman, M Spiropulu, J.R Vlimant, C Wang, S Xie, R.Y Zhu
California Institute of Technology, Pasadena, California, United States of America

J Alison, S An, M B Andrews, P Bryant, M Cremonesi, V Dutta, T Ferguson, A Harilal, C Liu, T Mudholkar, S Murthy, P Palit, M Paulini, A Roberts, A Sanchez, W Terrill
Carnegie Mellon University, Pittsburgh, Pennsylvania, United States of America

J P Cumalat, W T Ford, A Hart, A Hassani, G Karathanasis, E MacDonald, N Manganelli, A Perloff, C Savard, N Schonbeck, K Stenson, K A Ulmer, S R Wagner, N Zipper
University of Colorado Boulder, Boulder, Colorado, United States of America

J Alexander, S Bright-Thonney, X Chen, D J Cranshaw, J Fan, X Fan, D Gadkari, S Hogan, P Kotamnives, J Monroy, M Oshiro, J R Patterson, J Reichert, M Reid, A Ryd, J Thom, P Wittich, R Zou
Cornell University, Ithaca, New York, United States of America

M Albrow, M Alyari, O Amram, G Apollinari, A Apresyan, L A T Bauerdick, D Berry, J Berryhill, P C Bhat, K Burkett, J N Butler, A Canepa, G B Cerati, H W K Cheung, F Chlebana, G Cummings, J Dickinson, I Dutta, V D Elvira, Y Feng, J Freeman, A Gandrakota, Z Gecse, L Gray, D Green, A Grummer, S Grünendahl, D Guerrero, O Gutsche, R M Harris, R Heller, T C Herwig, J Hirschauer, L Horyn, B Jayatilaka, S Jindariani, M Johnson, U Joshi, T Klijnsma, B Klima, K H.M Kwok, S Lammel, D Lincoln, R Lipton, T Liu, C Madrid, K Maeshima, C Mantilla, D Mason, P McBride, P Merkel, S Mrenna, S Nahn, J Ngadiuba, D Noonan, V Papadimitriou, N Pastika, K Pedro, C Pena[85], F Ravera, A Reinsvold Hall[86], L Ristori, E Sexton-Kennedy, N Smith, A Soha, L Spiegel, S Stoynev, J Strait, L Taylor, S Tkaczyk, N V Tran, L Uplegger, E W Vaandering, I Zoi
Fermi National Accelerator Laboratory, Batavia, Illinois, United States of America

C Aruta, P Avery, D Bourilkov, L Cadamuro, P Chang, V Cherepanov, R D Field, E Koenig, M Kolosova, J Konigsberg, A Korytov, K H Lo, K Matchev, N Menendez, G Mitselmakher, K Mohrman, A Muthirakalayil Madhu, N Rawal, D Rosenzweig, S Rosenzweig, K Shi, J Wang
University of Florida, Gainesville, Florida, United States of America

T Adams, A Al Kadhim, A Askew, S Bower, R Habibullah, V Hagopian, R Hashmi, R.S Kim, S Kim, T Kolberg, G Martinez, H Prosper, P R Prova, M Wulansatiti, R Yohay, J Zhang
Florida State University, Tallahassee, Florida, United States of America

B Alsufyani, M M Baarmand, S Butalla, T Elkafrawy[20], M Hohlmann, R Kumar Verma, M Rahmani, E Yanes
Florida Institute of Technology, Melbourne, Florida, United States of America

M R Adams, A Baty, C Bennett, R Cavanaugh, R Escobar Franco, O Evdokimov, C E Gerber, D J Hofman, J h Lee, D S Lemos, A H Merrit, C Mills, S Nanda, G Oh, B Ozek, D Pilipovic, R Pradhan, T Roy, S Rudrabhatla, M B Tonjes, N Varelas, Z Ye, J Yoo
University of Illinois Chicago, Chicago, United States of America, Chicago, United States of America

M Alhusseini, D Blend, K Dilsiz[87], L Emediato, G Karaman, O K Köseyan, J -P Merlo, A Mestvirishvili[88], J Nachtman, O Neogi, H Ogul[89], Y Onel, A Penzo, C Snyder, E Tiras[90]
The University of Iowa, Iowa City, Iowa, United States of America

B Blumenfeld, L Corcodilos, J Davis, A V Gritsan, L Kang, S Kyriacou, P Maksimovic, M Roguljic, J Roskes, S Sekhar, M Swartz
Johns Hopkins University, Baltimore, Maryland, United States of America

A Abreu, L F Alcerro Alcerro, J Anguiano, P Baringer, A Bean, Z Flowers, D Grove, J King, G Krintiras, M Lazarovits, C Le Mahieu, C Lindsey, J Marquez, N Minafra, M Murray, M Nickel, M Pitt, S Popescu[91], C Rogan, C Royon, R Salvatico, S Sanders, C Smith, Q Wang, G Wilson
The University of Kansas, Lawrence, Kansas, United States of America

B Allmond, A Ivanov, K Kaadze, A Kalogeropoulos, D Kim, Y Maravin, K Nam, J Natoli, D Roy, G Sorrentino
Kansas State University, Manhattan, Kansas, United States of America

F Rebassoo, D Wright
Lawrence Livermore National Laboratory, Livermore, California, United States of America

A Baden, A Belloni, Y M Chen, S C Eno, N J Hadley, S Jabeen, R G Kellogg, T Koeth, Y Lai, S Lascio, A C Mignerey, S Nabili, C Palmer, C Papageorgakis, M M Paranjpe, L Wang
University of Maryland, College Park, Maryland, United States of America

J Bendavid, I A Cali, M D'Alfonso, J Eysermans, C Freer, G Gomez-Ceballos, M Goncharov, G Grosso, P Harris, D Hoang, D Kovalskyi, J Krupa, L Lavezzo, Y -J Lee, K Long, C Mironov, A Novak, C Paus, D Rankin, C Roland, G Roland, S Rothman, G S F Stephans, Z Wang, B Wyslouch, T J Yang
Massachusetts Institute of Technology, Cambridge, Massachusetts, United States of America

B Crossman, B M Joshi, C Kapsiak, M Krohn, D Mahon, J Mans, B Marzocchi, S Pandey, M Revering, R Rusack, R Saradhy, N Schroeder, N Strobbe, M A Wadud
University of Minnesota, Minneapolis, Minnesota, United States of America

L M Cremaldi
University of Mississippi, Oxford, Mississippi, United States of America

K Bloom, D R Claes, G Haza, J Hossain, C Joo, I Kravchenko, J E Siado, W Tabb, A Vagnerini, A Wightman, F Yan, D Yu
University of Nebraska-Lincoln, Lincoln, Nebraska, United States of America

H Bandyopadhyay, L Hay, I Iashvili, A Kharchilava, M Morris, D Nguyen, S Rappoccio, H Rejeb Sfar, A Williams
State University of New York at Buffalo, Buffalo, New York, United States of America

G Alverson, E Barberis, J Dervan, Y Haddad, Y Han, A Krishna, J Li, M Lu, G Madigan, R Mccarthy, D.M Morse, V Nguyen, T Orimoto, A Parker, L Skinnari, A Tishelman-Charny, B Wang, D Wood
Northeastern University, Boston, Massachusetts, United States of America

S Bhattacharya, J Bueghly, Z Chen, S Dittmer, K A Hahn, Y Liu, Y Miao, D G Monk, M H Schmitt, A Taliercio, M Velasco
Northwestern University, Evanston, Illinois, United States of America

G Agarwal, R Band, R Bucci, S Castells, A Das, R Goldouzian, M Hildreth, K W Ho, K Hurtado Anampa, T Ivanov, C Jessop, K Lannon, J Lawrence, N Loukas, L Lutton, J Mariano, N Marinelli, I Mcalister, T McCauley, C Mcgrady, C Moore, Y Musienko[16], H Nelson,

M Osherson, A Piccinelli, R Ruchti, A Townsend, Y Wan, M Wayne, H Yockey, M Zarucki, L Zygala
University of Notre Dame, Notre Dame, Indiana, United States of America

A Basnet, B Bylsma, M Carrigan, L S Durkin, C Hill, M Joyce, M Nunez Ornelas, K Wei, B.L Winer, B R Yates
The Ohio State University, Columbus, Ohio, United States of America

F M Addesa, H Bouchamaoui, P Das, G Dezoort, P Elmer, A Frankenthal, B Greenberg, N Haubrich, G Kopp, S Kwan, D Lange, A Loeliger, D Marlow, I Ojalvo, J Olsen, A Shevelev, D Stickland, C Tully
Princeton University, Princeton, New Jersey, United States of America

S Malik
University of Puerto Rico, Mayaguez, Puerto Rico, United States of America

A S Bakshi, V E Barnes, S Chandra, R Chawla, S Das, A Gu, L Gutay, M Jones, A W Jung, D Kondratyev, A M Koshy, M Liu, G Negro, N Neumeister, G Paspalaki, S Piperov, V Scheurer, J F Schulte, M Stojanovic, J Thieman, A K Virdi, F Wang, W Xie
Purdue University, West Lafayette, Indiana, United States of America

J Dolen, N Parashar, A Pathak
Purdue University Northwest, Hammond, Indiana, United States of America

D Acosta, T Carnahan, K M Ecklund, P J Fernández Manteca, S Freed, P Gardner, F J M Geurts, W Li, O Miguel Colin, B P Padley, R Redjimi, J Rotter, E Yigitbasi, Y Zhang
Rice University, Houston, Texas, United States of America

A Bodek, P de Barbaro, R Demina, J L Dulemba, A Garcia-Bellido, O Hindrichs, A Khukhunaishvili, N Parmar, P Parygin[92], E Popova[92], R Taus
University of Rochester, Rochester, New York, United States of America

K Goulianos
The Rockefeller University, New York, New York, United States of America

B Chiarito, J P Chou, Y Gershtein, E Halkiadakis, M Heindl, D Jaroslawski, O Karacheban[30], I Laflotte, A Lath, R Montalvo, K Nash, H Routray, S Salur, S Schnetzer, S Somalwar, R Stone, S A Thayil, S Thomas, J Vora, H Wang
Rutgers, The State University of New Jersey, Piscataway, New Jersey, United States of America

H Acharya, D Ally, A G Delannoy, S Fiorendi, S Higginbotham, T Holmes, A R Kanuganti, N Karunarathna, L Lee, E Nibigira, S Spanier
University of Tennessee, Knoxville, Tennessee, United States of America

D Aebi, M Ahmad, O Bouhali[93], R Eusebi, J Gilmore, T Huang, T Kamon[94], H Kim, S Luo, R Mueller, D Overton, D Rathjens, A Safonov
Texas A&M University, College Station, Texas, United States of America

N Akchurin, J Damgov, V Hegde, A Hussain, Y Kazhykarim, K Lamichhane, S W Lee, A Mankel, T Peltola, I Volobouev, A Whitbeck
Texas Tech University, Lubbock, Texas, United States of America

E Appelt, Y Chen, S Greene, A Gurrola, W Johns, R Kunnawalkam Elayavalli, A Melo, F Romeo, P Sheldon, S Tuo, J Velkovska, J Viinikainen
Vanderbilt University, Nashville, Tennessee, United States of America

B Cardwell, B Cox, J Hakala, R Hirosky, A Ledovskoy, C Neu, C E Perez Lara
University of Virginia, Charlottesville, Virginia, United States of America

P E Karchin
Wayne State University, Detroit, Michigan, United States of America

A Aravind, S Banerjee, K Black, T Bose, S Dasu, I De Bruyn, P Everaerts, C Galloni, H He, M Herndon, A Herve, C K Koraka, A Lanaro, R Loveless, J Madhusudanan Sreekala, A Mallampalli, A Mohammadi, S Mondal, G Parida, L Pétré, D Pinna, A Savin, V Shang, V Sharma, W H Smith, D Teague, H.F Tsoi, W Vetens, A Warden
University of Wisconsin - Madison, Madison, Wisconsin, United States of America

S Afanasiev, V Andreev, Yu Andreev, T Aushev, M Azarkin, A Babaev, A Belyaev, V Blinov[95], E Boos, V Borshch, D Budkouski, V Bunichev, V Chekhovsky, R Chistov[95], M Danilov[95], A Dermenev, T Dimova[95], D Druzhkin[96], M Dubinin[85], L Dudko, A Ershov, G Gavrilov, V Gavrilov, S Gninenko, V Golovtcov, N Golubev, I Golutvin, I Gorbunov, A Gribushin, Y Ivanov, V Kachanov, V Karjavine, A Karneyeu, V Kim[95], M Kirakosyan, D Kirpichnikov, M Kirsanov, V Klyukhin, O Kodolova[97],

V Korenkov, A Kozyrev[95], N Krasnikov, A Lanev, P Levchenko[98], N Lychkovskaya, V Makarenko, A Malakhov, V Matveev[95], V Murzin, A Nikitenko[99,97], S Obraztsov, V Oreshkin, V Palichik, V Perelygin, S Petrushanko, S Polikarpov[95], V Popov, O Radchenko[95], M Savina, V Savrin, V Shalaev, S Shmatov, S Shulha, Y Skovpen[95], S Slabospitskii, V Smirnov, A Snigirev, D Sosnov, V Sulimov, E Tcherniaev, A Terkulov, O Teryaev, I Tlisova, A Toropin, L Uvarov, A Uzunian, A Vorobyev†, N Voytishin, B S Yuldashev[100], A Zarubin, I Zhizhin, A Zhokin
Authors affiliated with an institute or an international laboratory covered by a cooperation agreement with CERN

† Deceased
[1]Also at Yerevan State University, Yerevan, Armenia
[2]Also at TU Wien, Vienna, Austria
[3]Also at Institute of Basic and Applied Sciences, Faculty of Engineering, Arab Academy for Science, Technology and Maritime Transport, Alexandria, Egypt
[4]Also at Ghent University, Ghent, Belgium
[5]Also at Universidade Estadual de Campinas, Campinas, Brazil
[6]Also at Federal University of Rio Grande do Sul, Porto Alegre, Brazil
[7]Also at UFMS, Nova Andradina, Brazil
[8]Also at Nanjing Normal University, Nanjing, People's Republic of China
[9]Now at The University of Iowa, Iowa City, Iowa, United States of America
[10]Also at University of Chinese Academy of Sciences, Beijing, People's Republic of China
[11]Also at People's Republic of China Center of Advanced Science and Technology, Beijing, People's Republic of China
[12]Also at University of Chinese Academy of Sciences, Beijing, People's Republic of China
[13]Also at People's Republic of China Spallation Neutron Source, Guangdong, People's Republic of China
[14]Now at Henan Normal University, Xinxiang, People's Republic of China
[15]Also at Université Libre de Bruxelles, Bruxelles, Belgium
[16]Also at an institute or an international laboratory covered by a cooperation agreement with CERN
[17]Also at Helwan University, Cairo, Egypt
[18]Now at Zewail City of Science and Technology, Zewail, Egypt
[19]Also at British University in Egypt, Cairo, Egypt
[20]Now at Ain Shams University, Cairo, Egypt
[21]Also at Purdue University, West Lafayette, Indiana, United States of America
[22]Also at Université de Haute Alsace, Mulhouse, France
[23]Also at Department of Physics, Tsinghua University, Beijing, People's Republic of China
[24]Also at The University of the State of Amazonas, Manaus, Brazil
[25]Also at Erzincan Binali Yildirim University, Erzincan, Turkey
[26]Also at University of Hamburg, Hamburg, Germany
[27]Also at RWTH Aachen University, III. Physikalisches Institut A, Aachen, Germany
[28]Also at Isfahan University of Technology, Isfahan, Iran
[29]Also at Bergische University Wuppertal (BUW), Wuppertal, Germany
[30]Also at Brandenburg University of Technology, Cottbus, Germany
[31]Also at Forschungszentrum Jülich, Juelich, Germany
[32]Also at CERN, European Organization for Nuclear Research, Geneva, Switzerland
[33]Also at Institute of Physics, University of Debrecen, Debrecen, Hungary
[34]Also at Institute of Nuclear Research ATOMKI, Debrecen, Hungary
[35]Now at Universitatea Babes-Bolyai - Facultatea de Fizica, Cluj-Napoca, Romania
[36]Also at Physics Department, Faculty of Science, Assiut University, Assiut, Egypt
[37]Also at HUN-REN Wigner Research Centre for Physics, Budapest, Hungary
[38]Also at Punjab Agricultural University, Ludhiana, India
[39]Also at University of Visva-Bharati, Santiniketan, India
[40]Also at Indian Institute of Science (IISc), Bangalore, India
[41]Also at Birla Institute of Technology, Mesra, Mesra, India
[42]Also at IIT Bhubaneswar, Bhubaneswar, India
[43]Also at Institute of Physics, Bhubaneswar, India
[44]Also at University of Hyderabad, Hyderabad, India
[45]Also at Deutsches Elektronen-Synchrotron, Hamburg, Germany
[46]Also at Department of Physics, Isfahan University of Technology, Isfahan, Iran
[47]Also at Sharif University of Technology, Tehran, Iran
[48]Also at Department of Physics, University of Science and Technology of Mazandaran, Behshahr, Iran
[49]Also at Italian National Agency for New Technologies, Energy and Sustainable Economic Development, Bologna, Italy
[50]Also at Centro Siciliano di Fisica Nucleare e di Struttura Della Materia, Catania, Italy
[51]Also at Università degli Studi Guglielmo Marconi, Roma, Italy
[52]Also at Scuola Superiore Meridionale, Università di Napoli 'Federico II', Napoli, Italy
[53]Also at Fermi National Accelerator Laboratory, Batavia, Illinois, United States of America
[54]Also at Consiglio Nazionale delle Ricerche - Istituto Officina dei Materiali, Perugia, Italy
[55]Also at Riga Technical University, Riga, Latvia
[56]Also at Department of Applied Physics, Faculty of Science and Technology, Universiti Kebangsaan Malaysia, Bangi, Malaysia
[57]Also at Consejo Nacional de Ciencia y Tecnología, Mexico City, Mexico

[58]Also at Trincomalee Campus, Eastern University, Sri Lanka, Nilaveli, Sri Lanka
[59]Also at Saegis Campus, Nugegoda, Sri Lanka
[60]Also at National and Kapodistrian University of Athens, Athens, Greece
[61]Also at Ecole Polytechnique Fédérale LaUnited States of Americanne, LaUnited States of Americanne, Switzerland
[62]Also at Universität Zürich, Zurich, Switzerland
[63]Also at Stefan Meyer Institute for Subatomic Physics, Vienna, Austria
[64]Also at Laboratoire d'Annecy-le-Vieux de Physique des Particules, IN2P3-CNRS, Annecy-le-Vieux, France
[65]Also at Near East University, Research Center of Experimental Health Science, Mersin, Turkey
[66]Also at Konya Technical University, Konya, Turkey
[67]Also at Izmir Bakircay University, Izmir, Turkey
[68]Also at Adiyaman University, Adiyaman, Turkey
[69]Also at Bozok Universitetesi Rektörlügü, Yozgat, Turkey
[70]Also at Marmara University, Istanbul, Turkey
[71]Also at Milli Savunma University, Istanbul, Turkey
[72]Also at Kafkas University, Kars, Turkey
[73]Now at stanbul Okan University, Istanbul, Turkey
[74]Also at Hacettepe University, Ankara, Turkey
[75]Also at Istanbul University - Cerrahpasa, Faculty of Engineering, Istanbul, Turkey
[76]Also at Yildiz Technical University, Istanbul, Turkey
[77]Also at Vrije Universiteit Brussel, Brussel, Belgium
[78]Also at School of Physics and Astronomy, University of Southampton, Southampton, United Kingdom
[79]Also at University of Bristol, Bristol, United Kingdom
[80]Also at IPPP Durham University, Durham, United Kingdom
[81]Also at Monash University, Faculty of Science, Clayton, Australia
[82]Also at Università di Torino, Torino, Italy
[83]Also at Bethel University, St. Paul, Minnesota, United States of America
[84]Also at Karamanoğlu Mehmetbey University, Karaman, Turkey
[85]Also at California Institute of Technology, Pasadena, California, United States of America
[86]Also at United States Naval Academy, Annapolis, Maryland, United States of America
[87]Also at Bingol University, Bingol, Turkey
[88]Also at Georgian Technical University, Tbilisi, Georgia
[89]Also at Sinop University, Sinop, Turkey
[90]Also at Erciyes University, Kayseri, Turkey
[91]Also at Horia Hulubei National Institute of Physics and Nuclear Engineering (IFIN-HH), Bucharest, Romania
[92]Now at an institute or an international laboratory covered by a cooperation agreement with CERN
[93]Also at Texas A&M University at Qatar, Doha, Qatar
[94]Also at Kyungpook National University, Daegu, Republic of Korea
[95]Also at another institute or international laboratory covered by a cooperation agreement with CERN
[96]Also at Universiteit Antwerpen, Antwerpen, Belgium
[97]Also at Yerevan Physics Institute, Yerevan, Armenia
[98]Also at Northeastern University, Boston, Massachusetts, United States of America
[99]Also at Imperial College, London, United Kingdom
[100]Also at Institute of Nuclear Physics of the Uzbekistan Academy of Sciences, Tashkent, Uzbekistan

References

[1] Budnev V M, Ginzburg I F, Meledin G V and Serbo V G 1973 The process pp $\to e^+e^-$ and the possibility of its calculation by means of quantum electrodynamics only *Nucl. Phys.* B **63** 519
[2] Adams J *et al* (STAR Collaboration) 2004 Production of e^+e^- pairs accompanied by nuclear dissociation in ultra-peripheral heavy ion collision *Phys. Rev.* C **70** 031902
[3] Abulencia A *et al* (CDF Collaboration) 2007 Observation of exclusive electron-positron production in hadron-hadron collisions *Phys. Rev. Lett.* **98** 112001
[4] Aaltonen T *et al* (CDF Collaboration) 2009 Observation of exclusive charmonium production and $\gamma\gamma \to \mu^+\mu^-$ in $p\bar{p}$ collisions at $\sqrt{s} = 1.96$ TeV *Phys. Rev. Lett.* **102** 242001
[5] Aaltonen T *et al* (CDF Collaboration) 2009 Search for exclusive Z boson production and observation of high mass $p\bar{p} \to \gamma\gamma \to p\ell\ell\bar{p}$ events in $p\bar{p}$ collisions at $\sqrt{s} = 1.96$ TeV *Phys. Rev. Lett.* **102** 222002
[6] Aad G *et al* (ATLAS Collaboration) 2021 Exclusive dimuon production in ultraperipheral Pb+Pb collisions at $\sqrt{s_{\mathrm{NN}}} = 5.02$ TeV with ATLAS *Phys. Rev.* C **104** 024906
[7] Chatrchyan S *et al* (CMS Collaboration) 2012 Search for exclusive or semi-exclusive photon pair production and observation of exclusive and semi-exclusive electron pair production in pp collisions at $\sqrt{s} = 7$ TeV *J. High Energy Phys.* JHEP11(2012)080
[8] Chatrchyan S *et al* (CMS Collaboration) 2012 Exclusive photon-photon production of muon pairs in proton-proton collisions at $\sqrt{s} = 7$ TeV *J. High Energy Phys.* JHEP01(2012)052
[9] Aad G *et al* (ATLAS Collaboration) 2023 Observation of the $\gamma\gamma \to \tau\tau$ process in Pb+Pb collisions and constraints on the τ-lepton anomalous magnetic moment with the ATLAS detector *Phys. Rev. Lett.* **131** 151802
[10] Tumasyan A *et al* (CMS Collaboration) 2023 Observation of τ lepton pair production in ultraperipheral lead-lead collisions at $\sqrt{s_{\mathrm{NN}}} = 5.02$ TeV *Phys. Rev. Lett.* **131** 151803
[11] del Aguila F, Cornet F and Illana J I 1991 The possibility of using a large heavy-ion collider for measuring the electromagnetic properties of the tau lepton *Phys. Lett.* B **271** 256
[12] Atag S and Billur A A 2010 Possibility of determining τ lepton electromagnetic moments in $\gamma\gamma \to \tau^+\tau^-$ process at the CERN-LHC *J. High Energy Phys.* JHEP11(2010)060
[13] Dyndal M, Klusek-Gawenda M, Schott M and Szczurek A 2020 Anomalous electromagnetic moments of τ lepton in $\gamma\gamma \to \tau^+\tau^-$ reaction in Pb+Pb collisions at the LHC *Phys. Lett.* B **809** 135682
[14] Beresford L and Liu J 2020 New physics and tau g-2 using LHC heavy ion collisions *Phys. Rev.* D **102** 113008
[15] Schwinger J 1948 On quantum-electrodynamics and the magnetic moment of the electron *Phys. Rev.* **73** 416
[16] Parker R H, Yu C, Zhong W, Estey B and Müller H 2018 Measurement of the fine-structure constant as a test of the standard model *Science* **360** 191
[17] Fan X, Myers T G, Sukra B A D and Gabrielse G 2023 Measurement of the electron magnetic moment *Phys. Rev. Lett.* **130** 071801

[18] Abi B *et al* (Muon g-2 Collaboration) 2021 Measurement of the positive muon anomalous magnetic moment to 0.46 ppm *Phys. Rev. Lett.* **126** 141801

[19] Aguillard D P *et al* (Muon g-2 Collaboration) 2023 Measurement of the positive muon anomalous magnetic moment to 0.20 ppm *Phys. Rev. Lett.* **131** 161802

[20] Aoyama T *et al* 2020 The anomalous magnetic moment of the muon in the standard model *Phys. Rep.* **887** 1

[21] Eidelman S and Passera M 2007 Theory of the tau lepton anomalous magnetic moment *Mod. Phys. Lett.* A **22** 159

[22] Yamaguchi Y and Yamanaka N 2020 Large long-distance contributions to the electric dipole moments of charged leptons in the standard model *Phys. Rev. Lett.* **125** 241802

[23] Crivellin A, Hoferichter M and Roney J M 2022 Toward testing the magnetic moment of the tau at one part per million *Phys. Rev.* D **106** 093007

[24] DELPHI Collaboration 2004 Study of tau-pair production in photon-photon collisions at LEP and limits on the anomalous electromagnetic moments of the tau lepton *Eur. Phys. J.* C **35** 159

[25] Ackerstaff K *et al* (OPAL Collaboration) 1998 An upper limit on the anomalous magnetic moment of the tau lepton *Phys. Lett.* B **431** 188

[26] Acciarri M *et al* (L3 Collaboration) 1998 Measurement of the anomalous magnetic and electric dipole moments of the tau lepton *Phys. Lett.* B **434** 169

[27] Inami K *et al* (Belle Collaboration) 2022 An improved search for the electric dipole moment of the τ lepton *J. High Energy Phys.* JHEP04(2022)110

[28] Albrecht H *et al* (ARGUS Collaboration) 2000 A search for the electric dipole moment of the tau lepton *Phys. Lett.* B **485** 37

[29] Chatrchyan S *et al* (CMS Collaboration) 2013 Study of exclusive two-photon production of W^+W^- in pp collisions at $\sqrt{s} = 7$ TeV and constraints on anomalous quartic gauge couplings *J. High Energy Phys.* JHEP07(2013)116

[30] Khachatryan V *et al* (CMS Collaboration) 2016 Evidence for exclusive $\gamma\gamma \to W^+W^-$ production and constraints on anomalous quartic gauge couplings in pp collisions at $\sqrt{s} = 7$ and 8 TeV *J. High Energy Phys.* JHEP08(2016)119

[31] Sirunyan A M *et al* (CMS and TOTEM Collaborations) 2018 Observation of proton-tagged, central (semi)exclusive production of high-mass lepton pairs in pp collisions at 13 TeV with the CMS-TOTEM precision proton spectrometer *J. High Energy Phys.* JHEP07(2018)153

[32] Aaboud M *et al* (ATLAS Collaboration) 2016 Measurement of exclusive $\gamma\gamma \to W^+W^-$ production and search for exclusive Higgs boson production in pp collisions at $\sqrt{s} = 8$ TeV using the ATLAS detector *Phys. Rev.* D **94** 032011

[33] Aad G *et al* (ATLAS Collaboration) 2021 Observation of photon-induced W^+W^- production in pp collisions at $\sqrt{s} = 13$ TeV using the ATLAS detector *Phys. Lett.* B **816** 136190

[34] The CMS collaboration 2024 HEPData record for this analysis (https://doi.org/10.17182/hepdata.152621)

[35] Chatrchyan S *et al* (CMS Collaboration) 2008 The CMS experiment at the CERN LHC *J. Instrum.* **3** S08004

[36] Sirunyan A M *et al* (CMS Collaboration) 2020 Performance of the CMS Level-1 trigger in proton-proton collisions at $\sqrt{s} = 13$ TeV *J. Instrum.* **15** 10017

[37] Khachatryan V *et al* (CMS Collaboration) 2017 The CMS trigger system *J. Instrum.* **12** 01020

[38] Shao H-S and d'Enterria D 2022 gamma-UPC: automated generation of exclusive photon-photon processes in ultraperipheral proton and nuclear collisions with varying form factors *J. High Energy Phys.* JHEP09(2022)24

[39] Alwall J *et al* 2014 The automated computation of tree-level and next-to-leading order differential cross sections and their matching to parton shower simulations *J. High Energy Phys.* JHEP07(2014)079

[40] Alwall J, Demin P, Visscher S D, Frederix R, Herquet M, Maltoni F, Plehn T, Rainwater D L and Stelzer T 2007 MadGraph/MadEvent v4: the new web generation *J. High Energy Phys.* JHEP09(2007)028

[41] Frederix R and Frixione S 2012 Merging meets matching in MC@NLO *J. High Energy Phys.* JHEP12(2012)061

[42] Shao H-S and d'Enterria D 2024 Dimuon and ditau production in photon-photon collisions at next-to-leading order in QED (arXiv:2407.13610v1 [hep-ph])

[43] Harland-Lang L A, Tasevsky M, Khoze V A and Ryskin M G 2020 A new approach to modelling elastic and inelastic photon-initiated production at the LHC: SuperChic 4 *Eur. Phys. J.* C **80** 925

[44] Brivio I, Jiang Y and Trott M 2017 The SMEFTsim package, theory and tools *J. High Energy Phys.* JHEP12(2017)070

[45] Brivio I 2021 SMEFTsim 3.0—a practical guide *J. High Energy Phys.* JHEP04(2021)073

[46] Artoisenet P, Lemaitre V, Maltoni F and Mattelaer O 2010 Automation of the matrix element reweighting method *J. High Energy Phys.* JHEP12(2010)068

[47] Nason P 2004 A new method for combining NLO QCD with shower Monte Carlo algorithms *J. High Energy Phys.* JHEP11(2007)070

[48] Frixione S, Nason P and Oleari C 2007 Matching NLO QCD computations with parton shower simulations: the POWHEG method *J. High Energy Phys.* JHEP11(2007)070

[49] Alioli S, Nason P, Oleari C and Re E 2010 A general framework for implementing NLO calculations in shower Monte Carlo programs: the POWHEG BOX *J. High Energy Phys.* JHEP06(2010)043

[50] Alioli S, Hamilton K, Nason P, Oleari C and Re E 2011 Jet pair production in POWHEG *J. High Energy Phys.* JHEP04(2011)081

[51] Alioli S, Nason P, Oleari C and Re E 2009 NLO Higgs boson production via gluon fusion matched with shower in POWHEG *J. High Energy Phys.* JHEP04(2009)002

[52] Sjöstrand T, Ask S, Christiansen J R, Corke R, Desai N, Ilten P, Mrenna S, Prestel S, Rasmussen C O and Skands P Z 2015 An introduction to PYTHIA 8.2 *Comput. Phys. Commun.* **191** 159

[53] Sirunyan A M *et al* (CMS Collaboration) 2020 Extraction and validation of a new set of CMS PYTHIA8 tunes from underlying-event measurements *Eur. Phys. J.* C **80** 4

[54] Ball R D, Bertone V, Cerutti F, Del Debbio L, Forte S, Guffanti A, Latorre J I, Rojo J and Ubiali M 2012 Unbiased global determination of parton distributions and their uncertainties at NNLO and at LO *Nucl. Phys.* B **855** 153

[55] Ball R D, Bertone V, Carrazza S, Del Debbio L, Forte S, Guffanti A, Hartland NP and Rojo J (NNPDF Collaboration) 2013 Parton distributions with QED corrections *Nucl. Phys.* B **877** 290

[56] Ball R D *et al* (NNPDF Collaboration) 2017 Parton distributions from high-precision collider data *Eur. Phys. J.* C **77** 663

[57] Agostinelli S *et al* (GEANT4 Collaboration) 2003 GEANT4 — a simulation toolkit *Nucl. Instrum. Meth.* A **506** 250

[58] Sirunyan A M *et al* (CMS Collaboration) 2017 Particle-flow reconstruction and global event description with the CMS detector *J. Instrum.* **12** 10003

[59] Sirunyan A M *et al* (CMS Collaboration) 2021 Electron and photon reconstruction and identification with the CMS experiment at the CERN LHC *J. Instrum.* **16** 05014

[60] CMS Collaboration 2020 ECAL 2016 refined calibration and Run2 summary plots CMS Detector Performance Note CMS-DP-2020-021 (available at: https://cds.cern.ch/record/2717925)
[61] Sirunyan A M *et al* (CMS Collaboration) 2018 Performance of the CMS muon detector and muon reconstruction with proton-proton collisions at $\sqrt{s} = 13$ TeV *J. Instrum.* **13** 06015
[62] Sirunyan A M *et al* (CMS Collaboration) 2018 Performance of reconstruction and identification of τ leptons decaying to hadrons and ν_τ in pp collisions at $\sqrt{s} = 13$ TeV *J. Instrum.* **13** 10005
[63] Sirunyan A M *et al* (CMS Collaboration) 2022 Identification of hadronic tau lepton decays using a deep neural network *J. Instrum.* **17** 07023
[64] Sirunyan A M *et al* (CMS Collaboration) 2019 Performance of missing transverse momentum reconstruction in proton-proton collisions at $\sqrt{s} = 13$ TeV using the CMS detector *J. Instrum.* **14** 07004
[65] CMS Collaboration 2014 Description and performance of track and primary-vertex reconstruction with the CMS tracker *J. Instrum.* **9** 10009
[66] Adam W *et al* (Tracker Group of the CMS Collaboration) 2021 The CMS phase-1 pixel detector upgrade *J. Instrum.* **16** 02027
[67] CMS Collaboration 2020 Track impact parameter resolution for the full pseudo rapidity coverage in the 2017 dataset with the CMS phase-1 pixel detector CMS Detector Performance Note CMS-DP-2020-049 (available at: https://cds.cern.ch/record/27437 40)
[68] CMS Collaboration 2024 Performance of the CMS electromagnetic calorimeter in pp collisions at $\sqrt{s} = 13$ TeV Submitted to JINST (arXiv:2403.15518)
[69] Sirunyan A M *et al* (CMS Collaboration) 2021 Precision luminosity measurement in proton-proton collisions at $\sqrt{s} = 13$ TeV in 2015 and 2016 at CMS *Eur. Phys. J.* C **81** 800
[70] CMS Collaboration 2018 CMS luminosity measurement for the 2017 data-taking period at $\sqrt{s} = 13$ TeV CMS Physics Analysis Summary CMS-PAS-LUM-17-004 (available at: https://cds.cern.ch/record/2621960/)
[71] CMS Collaboration 2019 CMS luminosity measurement for the 2018 data-taking period at $\sqrt{s} = 13$ TeV CMS Physics Analysis Summary CMS-PAS-LUM-18-002 (available at: https://cds.cern.ch/record/2676164/)
[72] Gavin R, Li Y, Petriello F and Quackenbush S 2013 W physics at the LHC with FEWZ 2.1 *Comput. Phys. Commun.* **184** 208
[73] Barlow R and Beeston C 1993 Fitting using finite Monte Carlo samples *Comput. Phys. Commun.* **77** 219
[74] Sirunyan A M *et al* (CMS Collaboration) 2018 Measurement of the inelastic proton-proton cross section at $\sqrt{s} = 13$ TeV *J. High Energy Phys.* JHEP07(2018)161
[75] CMS Collaboration 2024 The CMS statistical analysis and combination tool: COMBINE (arXiv:2404.06614)
[76] Cowan G, Cranmer K, Gross E and Vitells O 2011 Asymptotic formulae for likelihood-based tests of new physics *Eur. Phys. J.* C **71** 1554